Multichannel Deconvolution of Layered Media Using Markov Chain Monte Carlo Methods

Idan Ram

Multichannel Deconvolution of Layered Media Using Markov Chain Monte Carlo Methods

Research Thesis

Submitted in Partial Fulfillment of the
Requirements for the Degree of
Master of Science in Electrical Engineering

Idan Ram

Submitted to the Senate of the Technion - Israel Institute of Technology
Nisan 5769 Haifa April 2009

The Research Thesis Was Done Under The Supervision of Assoc. Prof. Israel Cohen and Prof. Shalom Raz in the Faculty of Electrical Engineering.

Acknowledgement

I wish to express my gratitude to my advisors, Prof. Israel Cohen and Prof. Shalom Raz , for their guidance and support throughout all stages of this research. I would also like to thank my wife Sigal for her love and support.

THE GENEROUS FINANCIAL HELP OF THE TECHNION IS GRATEFULLY ACKNOWLEDGED.

Contents

List of Figures

List of Tables

Abstract

Multichannel seismic deconvolution is employed when the structure of the earth is estimated by transmitting an acoustic wave into the ground and measuring the reflected energy resulting from impedance changes. The observed seismic data can be modeled as a convolution between a two-dimensional (2D) reflectivity section and a one-dimensional (1D) seismic pulse (wavelet), which have been further degraded by additive noise. Deconvolution is used to remove the effect of the wavelet and produce an increased resolution estimate of the reflectivity where closely spaced reflectors can be identified. In this thesis we propose two multichannel blind deconvolution algorithms for the restoration of 2D seismic data. Both algorithms are based on a 2D reflectivity prior model, and use iterative multichannel deconvolution procedures which deconvolve the seismic data, while taking into account the spatial dependency between neighboring traces. The first algorithm employs in each iteration a modified maximum posterior mode (MPM) algorithm which estimates a reflectivity column from the corresponding observed trace using the estimate of the preceding reflectivity column. The second algorithm takes into account estimates of both the preceding and subsequent columns in the estima-

tion process. Both algorithms are applied to synthetic and real data and demonstrate better results compared to those obtained by a single-channel deconvolution method. The second algorithm which utilizes more information in the estimation process of each reflectivity column is shown to produce better results than the first algorithm.

List of Papers

The following paper have been submitted for publication on the results of some of the work described in this thesis:

I. Ram, I. Cohen and S. Raz "Multichannel Deconvolution of Seismic Signals Using Statistical MCMC Methods"

Glossary

Abbreviations

1D	One-Dimensional
2D	Two-Dimensional
BG	Bernoulli-Gaussian
SMLR	Single Most Likely Replacement
IWM	Iterated Window Maximization
MCMC	Markov Chain Monte Carlo
SEM	Stochastic Expectation Maximization
MPM	Maximum Posterior Mode
MBG	Markov Bernoulli Gaussian
MBRF	Markov Bernoulli Random Fields
MAP	Maximum A Posteriori
AR	Autoregressive
SC	Single-channel
MC	Multi-Channel

Alphabetic Symbols:

$\mathbf{h}$	Seismic wavelet
N_h	The length of the seismic wavelet $\mathbf{h}$
$\mathbf{r}$	Single-channel reflectivity sequence
N_r	Number of rows in the reflectivity
$\mathbf{w}$	Single-channel noise vector
$\mathbf{y}$	Single-channel seismic trace
N_y	Number of rows in the seismic data
$h(k)$	kth sample of the seismic wavelet
$r(k)$	kth reflector of $\mathbf{r}$
$w(k)$	kth sample of $\mathbf{w}$
$y(k)$	kth sample of $\mathbf{y}$
σ_w^2	Noise variance
$\mathbf{q}$	Bernoulli state vector characterizing the single-channel BG reflectivity
$q(k)$	kth sample of $\mathbf{q}$
$B(\alpha)$	Bernoulli distribution with parameter α.
λ	Probability for the presence of a reflector in the reflectivity
σ_r^2	Variance of the reflectors amplitude
$\boldsymbol{\theta}$	Vector of the missing parameters $\mathbf{h}, \lambda, \sigma_r, \sigma_w$
$\hat{\boldsymbol{\theta}}$	Vector of estimates of the missing parameters $\hat{\mathbf{h}}, \hat{\lambda}, \hat{\sigma}_r, \hat{\sigma}_w$
$\underline{\mathrm{Q}}$	Diagonal matrix with the elements of $\mathbf{q}$ on its diagonal
$\underline{\mathrm{H}}$	Convolution matrix associated with $\mathbf{h}$
$\underline{\mathrm{R}}$	Convolution matrix associated with $\mathbf{r}$

$\mathbf{r}_{-k}$	The vector $\mathbf{r}$ aside from its kth sample
$\mathbf{q}_{-k}$	The vector $\mathbf{q}$ aside from its kth sample
λ_k	Bernoulli parameter of the conditional distribution of $q(k)$
$m_{1,}V_1$	Mean and Variance of the Gaussian function in the conditional distribution of $r(k)$
m_w	Parameter used in the calculation of $m_1, m_{k,j}^b, m_{k,j}^f$ and $m_{k,j}^m$
V_w	Parameter used in the calculation of $m_1, V_1, m_{k,j}^b, V_{k,j}^b, m_{k,j}^f, V_{k,j}^f, m_{k,j}^m$ and $V_{k,j}^m$
E_h	Energy of the seismic wavelet
δ	Dirac's delta function
I_0	Number of iterations in the learning period of the Gibbs sampler
I	Total number of iterations of the Gibbs sampler
$\mathbf{r}^{(i)}, \mathbf{q}^{(i)}$	The ith samples of $\mathbf{r}$ and $\mathbf{q}$ produced by a Gibbs sampler
$\hat{\boldsymbol{\theta}}^{(i)}$	Vector of estimates $\hat{\mathbf{h}}^{(i)}, \hat{\lambda}^{(i)}, \hat{\sigma}_r^{(i)}, \hat{\sigma}_w^{(i)}$ produced in the ith iteration of the SEM algorithm
$\hat{\mathbf{r}}, \hat{\mathbf{q}}$	Estimates of $\mathbf{r}$ and $\mathbf{q}$
$\hat{r}(k), \hat{q}(k)$	kth samples of $\hat{\mathbf{r}}$ and $\hat{\mathbf{q}}$
$\mathbf{Y}$	2D seismic data
$\mathbf{y}_j$	The jth column of $\mathbf{Y}$
J	Number of columns in the 2D seismic data
$\mathbf{R}$	2D reflectivity section
$\mathbf{r}_j$	The jth column of $\mathbf{R}$
$r_{k,j}$	The kth sample in $\mathbf{r}_j$
$\mathbf{Q}$	2D location variables matrix

$\mathbf{q}_j$	The jth column of $\mathbf{Q}$
$q_{k,j}$	The kth sample in $\mathbf{q}_j$
$\mathbf{W}$	2D noise matrix
$\mathbf{w}_j$	The jth column of $\mathbf{W}$
$\mathbf{T}^{/}$	2D ascending transition variables matrix
$\mathbf{T}^{-}$	2D horizontal transition variables matrix
$\mathbf{T}^{\backslash}$	2D descending transition variables matrix
$\mathbf{t}^{/}_{j-1}, \mathbf{t}^{-}_{j-1}, \mathbf{t}^{\backslash}_{j-1}$	The $j-1$th columns of $\mathbf{T}^{/}, \mathbf{T}^{-}$ and $\mathbf{T}^{\backslash}$
$t^{/}_{k,j-1}, t^{-}_{k,j-1}, t^{\backslash}_{k,j-1}$	The kth samples in $\mathbf{t}^{/}_{j-1}, \mathbf{t}^{-}_{j-1}, \mathbf{t}^{\backslash}_{j-1}$
$\mu^{/}$	Bernoulli parameter of the ascending transition variable
μ^{-}	Bernoulli parameter of the horizontal transition variable
$\mu^{\backslash}$	Bernoulli parameter of the descending transition variable
ε	Probability for a discontinuity along a layer boundary
a	Parameter which controls the correlation between reflectors
w_r	Gaussian noise with zero mean and variance $(1-a^2)\,\sigma_r^2$
$\boldsymbol{\theta}_{MBG}$	The parameters $\left(a, \mu^{/}, \mu^{-}, \mu^{\backslash}, \varepsilon\right)$ of the MBG I model
$\hat{\boldsymbol{\theta}}_j$	An estimate of $\boldsymbol{\theta}$ obtained from $\mathbf{y}_j$
$\hat{\mathbf{R}}^{c}_{TBT}$	An estimate of $\mathbf{R}$ which is used in the calculation $\boldsymbol{\theta}_{MBG}$
$I^{/}$, I^{-}, $I^{\backslash}$	Number of positions in $\hat{\mathbf{R}}_{TBT}$ in which the orientation of the layer boundaries is upward, horizontal and downward
$\hat{\mu}^{/}$, $\hat{\mu}^{-}$, $\hat{\mu}^{-}$	Estimates of $\mu^{/}$, μ^{-} and $\mu^{\backslash}$
$\hat{\varepsilon}$	Estimate of ε
I_l	the number of layer boundaries in $\hat{\mathbf{R}}_{TBT}$

$\mathbf{l}_m$	The reflectors of the mth boundary in $\hat{\mathbf{R}}_{TBT}$ arranged in a vector
$l_m(k)$	The kth sample of $\mathbf{l}_m$
L_m	The length of $\mathbf{l}_m$
$\hat{a}_{YW}$	An estimate of a using Yule Walker equations
$\hat{a}$	An estimate of a
$\hat{\mathbf{R}}, \hat{\mathbf{Q}}, \hat{\mathbf{T}}^{/}, \hat{\mathbf{T}}^{-}, \hat{\mathbf{T}}^{\backslash}$	Estimates of $\mathbf{R}, \mathbf{Q}, \mathbf{T}^{/}, \mathbf{T}^{-}$ and $\mathbf{T}^{\backslash}$
$\hat{\mathbf{r}}_j, \hat{\mathbf{q}}_j, \hat{\mathbf{t}}^{/}_{j-1}, \hat{\mathbf{t}}^{-}_{j-1}, \hat{\mathbf{t}}^{\backslash}_{j-1}$	Estimates of $\mathbf{r}_j, \mathbf{q}_j, \mathbf{t}^{/}_{j-1}, \mathbf{t}^{-}_{j-1}$ and $\mathbf{t}^{\backslash}_{j-1}$
$\hat{r}_{k,j}, \hat{q}_{k,j}, \hat{t}^{/}_{k,j-1}, \hat{t}^{-}_{k,j-1}, \hat{t}^{\backslash}_{k,j-1}$	kth sample of $\hat{\mathbf{r}}_j, \hat{\mathbf{q}}_j, \hat{\mathbf{t}}^{/}_{j-1}, \hat{\mathbf{t}}^{-}_{j-1}, \hat{\mathbf{t}}^{\backslash}_{j-1}$
$\mathbf{r}_{-k,j}$	The vector $\mathbf{r}_j$ aside from its kth sample
$\mathbf{q}_{-k,j}$	The vector $\mathbf{q}_j$ aside from its kth sample
$\mathbf{t}^{/}_{-k,j-1}, \mathbf{t}^{-}_{-k,j-1}, \mathbf{t}^{\backslash}_{-k,j-1}$	The vectors $\mathbf{t}^{/}_{j-1}, \mathbf{t}^{-}_{j-1}, \mathbf{t}^{\backslash}_{j-1}$ aside from their kth samples
$\mu^{/}_{k,j-1}$, $\mu^{-}_{k,j-1}$, $\mu^{\backslash}_{k,j-1}$	Bernoulli parameter of conditional distributions of $t^{/}_{k,j-1}$, $t^{-}_{k,j-1}$ and $t^{-}_{k,j-1}$
$\lambda^{b}_{k,j}, \lambda^{f}_{k,j}, \lambda^{m}_{k,j}$	Bernoulli parameter of conditional distributions of $q_{k,j}$
$m^{b}_{k,j}, m^{f}_{k,j}, m^{m}_{k,j}$	Mean of the Gaussian functions in conditional distributions of $r(k)$
$V^{b}_{k,j}, V^{f}_{k,j}, V^{m}_{k,j}$	Variance of the Gaussian functions in conditional distributions of $r(k)$
$\mathbf{r}^{(i)}_j, \mathbf{q}^{(i)}_j, \mathbf{t}^{/\,(i)}_{j-1}, \mathbf{t}^{-\,(i)}_{j-1}, \mathbf{t}^{\backslash\,(i)}_{j-1}$	The ith samples of $\mathbf{r}_j, \mathbf{q}_j, \mathbf{t}^{/}_{j-1}, \mathbf{t}^{-}_{j-1}, \mathbf{t}^{\backslash}_{j-1}$ produced by a Gibbs sampler
$\left\|\cdot\right\|_1$	L_1 norm
$\left\|\cdot\right\|_2$	L_2 norm

N^{miss}, N_2^{miss}	
N^{false}, N_2^{false}	Measures of false and missed detections in an estimate of a 1D reflectivity sequence
$L^{miss+false}$, L^{miss}, L^{false}, $L_2^{miss+false}$, L_2^{miss}, L_2^{false}, L^{SSQ}	Loss functions used to quantify the performance of deconvolution algorithms
D	Difference measure used in the calculation of $L_2^{miss+false}$, $L_2^{miss}$and L_2^{false}
$\bar{\mathbf{r}}_j$	Vector concatenation of $\mathbf{r}_j$ and $\mathbf{r}_{j+1}$
$\bar{\mathbf{q}}_j$	Vector concatenation of $\mathbf{q}_j$ and $\mathbf{q}_{j+1}$
$\bar{\mathbf{t}}_{j-1}^{/}$	Vector concatenation of $\mathbf{t}_{j-1}^{/}$ and $\mathbf{t}_j^{/}$
$\bar{\mathbf{t}}_{j-1}^{-}$	Vector concatenation of $\mathbf{t}_{j-1}^{-}$ and $\mathbf{t}_j^{-}$
$\bar{\mathbf{t}}_{j-1}^{\backslash}$	Vector concatenation of $\mathbf{t}_{j-1}^{\backslash}$ and $\mathbf{t}_j^{\backslash}$
$\mathbf{t}_0^{/}$, $\mathbf{t}_0^{-}$, $\mathbf{t}_0^{/}$, $\mathbf{0}_{N_r\times 1}$	Vectors of N_r zeros
$\bar{\mathbf{r}}_j^{(i)}, \bar{\mathbf{q}}_j^{(i)}, \bar{\mathbf{t}}_{j-1}^{/\,(i)}, \bar{\mathbf{t}}_{j-1}^{-\,(i)}, \bar{\mathbf{t}}_{j-1}^{\backslash\,(i)}$	The ith samples of $\bar{\mathbf{r}}_j, \bar{\mathbf{q}}_j, \bar{\mathbf{t}}_{j-1}^{/}, \bar{\mathbf{t}}_{j-1}^{-}, \bar{\mathbf{t}}_{j-1}^{\backslash}$ produced by a Gibbs sampler
$\widehat{\bar{\mathbf{t}}}_{j-1}^{/}$, $\widehat{\bar{\mathbf{t}}}_{j-1}^{-}$, $\widehat{\bar{\mathbf{t}}}_{j-1}^{\backslash}$	Estimates of $\bar{\mathbf{t}}_{j-1}^{/}$, $\bar{\mathbf{t}}_{j-1}^{-}$ and $\bar{\mathbf{t}}_{j-1}^{\backslash}$
$\widehat{\bar{\mathbf{r}}}_j, \widehat{\bar{\mathbf{q}}}_j, \widehat{\bar{\mathbf{t}}}_{j-1}^{/}$, $\widehat{\bar{\mathbf{t}}}_{j-1}^{-}$, $\widehat{\bar{\mathbf{t}}}_{j-1}^{\backslash}$	Estimates of $\bar{\mathbf{r}}_j, \bar{\mathbf{q}}_j, \bar{\mathbf{t}}_{j-1}^{/}, \bar{\mathbf{t}}_{j-1}^{-}$ and $\bar{\mathbf{t}}_{j-1}^{\backslash}$
$\widehat{\bar{r}}_{k,j}, \widehat{\bar{q}}_{k,j}, \widehat{\bar{t}}_{k,j-1}^{/}, \widehat{\bar{t}}_{k,j-1}^{-}, \widehat{\bar{t}}_{k,j-1}^{\backslash}$	kth sample of $\widehat{\bar{\mathbf{r}}}_j, \widehat{\bar{\mathbf{q}}}_j, \widehat{\bar{\mathbf{t}}}_{j-1}^{/}$, $\widehat{\bar{\mathbf{t}}}_{j-1}^{-}$, $\widehat{\bar{\mathbf{t}}}_{j-1}^{\backslash}$
$\lambda_{k,j}^t$	Conditional probability used in the calculation of $\lambda_{k,j}^b$
$\eta_0^{/}$, $\eta_1^{/}, \rho_0^{/}$, $\rho_1^{/}$	Conditional probabilities used in the calculation of $\mu_{k,j-1}^{/}$
η_0^{-}, η_1^{-}, ρ_0^{-}, ρ_1^{-}	Conditional probabilities used in the calculation of $\mu_{k,j-1}^{-}$

$\eta_0^{\setminus}$, $\eta_1^{\setminus}$, $\rho_0^{\setminus}$, $\rho_1^{\setminus}$	Conditional probabilities used in the calculation of $\mu_{k,j-1}^{\setminus}$
g_0, g_1	Probabilities used in the calculation of $\lambda_{k,j}^f$
c_0, c_1	Probabilities used in the calculation of $\lambda_{k,j}^m$
a_{dk}	Parameter used in used in the calculation of $m_{k,j}^f, m_{k,j}^m, V_{k,j}^f, V_{k,j}^m, \lambda_{k,j}^f$ and $\lambda_{k,j}^m$
$m_{k,j}, \sigma_{k,j}^2$	Parameters used in used in the calculation of $m_{k,j}^b, m_{k,j}^m, V_{k,j}^b, V_{k,j}^m, \lambda_{k,j}^b$ and $\lambda_{k,j}^m$

Chapter 1

Introduction

1.1 Background

Multichannel seismic deconvolution is employed when the structure of the earth is estimated by transmitting an acoustic wave into the ground and measuring the reflected energy resulting from impedance changes. Under simplifying assumptions, the observations constructed from the reflected waves can be modeled as a convolution between a two-dimensional (2D) reflectivity section and a one-dimensional (1D) seismic pulse (wavelet), which have been further degraded by additive noise. Here we assume that the ground contains several homogenous, continuous and roughly horizontal layers. As a result, the 2D reflectivity section will be continuous, and will consist of layer boundaries which form smooth lines with a preferential orientation in the horizontal direction. The wavelet is a 1D vertical signal which represents the waveshape that scatters through the medium, and assumed common to all traces. An example of 2D synthetic seismic data and the reflectivity

section and seismic wavelet used for its creation can be seen in Fig. 1.1(a), (b) and (c), respectively. Since the recorded trace is a smeared version of the reflectivity, deconvolution is used to remove the effect of the wavelet and produce an increased resolution estimate of the reflectivity, where closely spaced reflectors can be identified. The seismic wavelet is usually unknown because of various effects such as high-frequency absorption and receiver ghosting, thus blind deconvolution must be applied in order to recover both the reflectivity and the wavelet.

Many methods utilize the fact that the wavelet is a 1D vertical signal and break the multichannel deconvolution problem into independent vertical 1D deconvolution problems. A 1D reflectivity column appears in the vertical direction as a sparse spike train where each spike (reflector) corresponds to a boundary between two adjacent homogenous layers. Mendel et al. [1], [2] use an autoregressive moving average model for the wavelet and model the reflectivity as a Bernoulli-Gaussian (BG) process [3], [4]. For each sample of the reflectivity sequence, a Bernoulli variable characterizes the presence or the absence of a reflector, and the amplitude of the reflector follows a Gaussian distribution when the Bernoulli variable is nonzero. They use second order statistics methods to estimate the wavelet and recover the reflectivity by maximum likelihood estimation. The maximum likelihood criterion is maximized using the Single Most Likely Replacement (SMLR) algorithm [2], which improves the likelihood by iteratively choosing a reflectivity sequence that varies at each iteration by only one sample. Kaaresen and Taxt [5] introduced an algorithm which alternately estimates a finite impulse response wavelet and a BG reflectivity. The wavelet is estimated using a least-squares fit

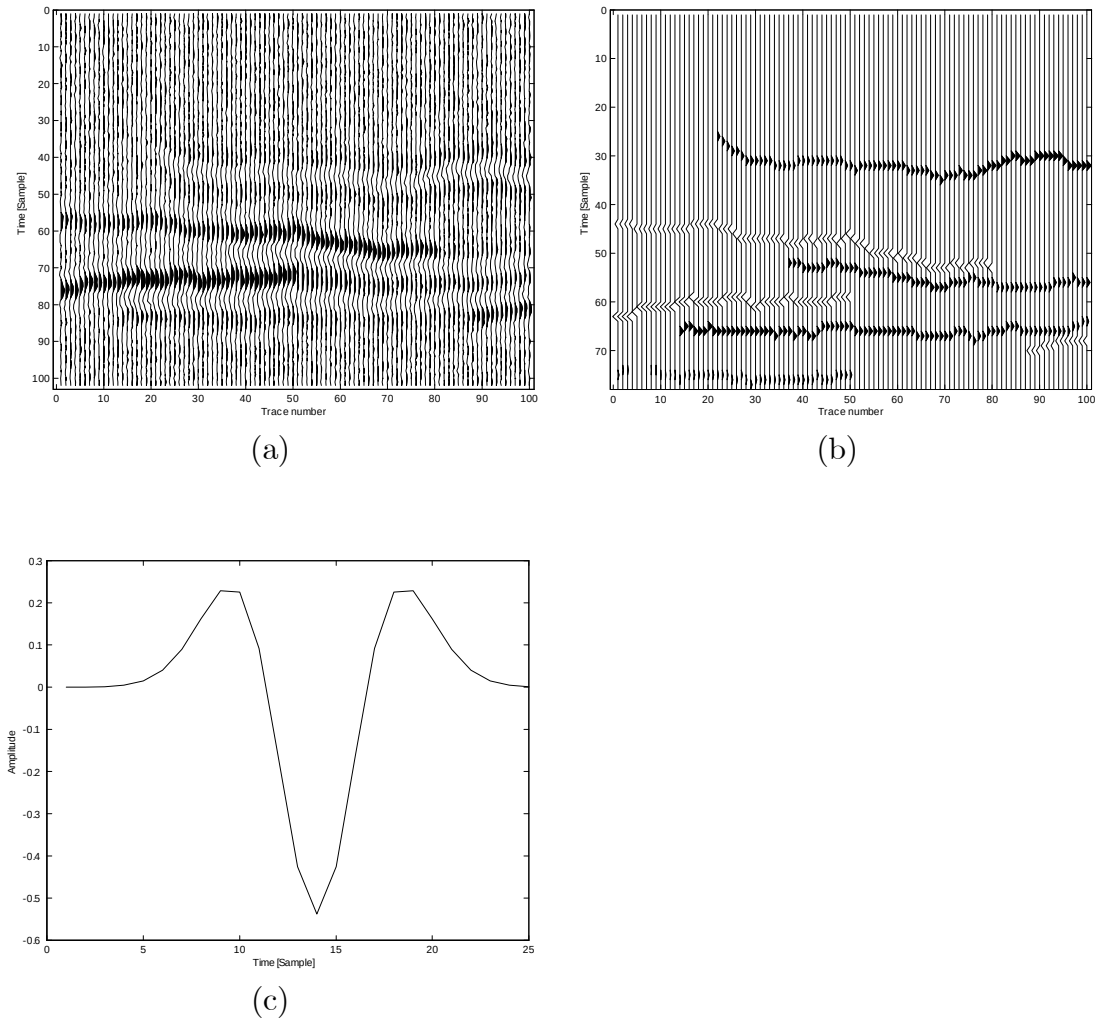

Figure 1.1: Example of synthetic seismic data: (a) 2D seismic data. (b) 2D reflectivity section, where black and white triangles denote postive and negative reflectors, respectively. (c) Seismic wavelet.

and the reflectivity is recovered using the iterated window maximization (IWM) algorithm [6]. The IWM algorithm is similar to the SMLR, but produces better results since it updates many samples at each step instead of only one. Cheng, Chen and Li [7] simultaneously estimate a BG reflectivity and a moving average wavelet using a Bayesian framework in which prior information is imposed on the seismic wavelet, BG reflectivity parameters and the noise variance. These parameters along with the reflectivity sequence are estimated using a Markov Chain Monte Carlo (MCMC) method called a Gibbs sampler [8], [9]. Rosec et al. [10] use a moving average wavelet and model the reflectivity sequence as a mixture of Gaussian distributions [11]. They propose two parameter estimation methods. The first method performs maximum likelihood estimation and use the stochastic expectation maximization (SEM) algorithm [12], [13] to maximize the likelihood criterion. The second method performs Bayesian estimation similarly to the method of Cheng, Chen and Li. The estimated parameters are employed by the maximum posterior mode (MPM) algorithm [14], which uses realizations of the reflectivity simulated by a Gibbs sampler to estimate the reflectivity.

Application of 1D restoration methods to 2D seismic data is clearly suboptimal, as it does not take into account the dependency between neighboring columns of the seismic data (traces), which stems from the continuous and roughly horizontal structure of the layers of the earth. Idier and Goussard [15] proposed two versions of a multichannel deconvolution method which takes into account the stratification of the layers. The two versions are based on two 2D reflectivity models: Markov-Bernoulli-Gaussian (MBG) I and II. Each model is composed

of a Markov-Bernoulli random field (MBRF) [16], which controls the geometrical characteristics of the reflectivity, and an amplitude field, defined conditionally to the MBRF. The deconvolution is carried out using a suboptimal maximum a posteriori (MAP) estimator, which iteratively recovers the columns of the reflectivity section. Each reflectivity column is estimated from the corresponding observed trace and the estimate of the previous reflectivity column, using an SMLR-type method. Kaaresen and Taxt [5] also suggest a multichannel version of their blind deconvolution algorithm, which accounts for the dependencies across the traces. However, this method encourages spatial continuity of the estimated reflectors using an optimization criterion which penalizes unwanted or unlikely configurations. Heimer, Cohen and Vassiliou [17], [18] introduced a multichannel blind deconvolution method which combines the algorithm of Kaaresen and Taxt and dynamic programming [19], [20] to find continuous paths of reflectors across the channels of the reflectivity section. However, layer discontinuities are not taken into account by this method. Heimer and Cohen [21] also proposed a multichannel blind deconvolution algorithm which is based on the MBG I reflectivity model. They first define a set of reflectivity states and legal transitions between configurations of neighboring reflectivity columns. Then they apply the Viterbi algorithm [22] for finding the most likely sequences of reflectors that are connected across the reflectivity section by legal transitions.

1.2 Motivation and Goals

Rosec et al. propose in [10] a single-channel blind deconvolution method. This method uses the SEM algorithm or a Bayesian framework to estimate the missing wavelet, noise variance and BG reflectivity parameters from a 1D seismic trace. Then it employs the obtained parameters to deconvolve this trace using the MPM algorithm. In order to recover a 2D reflectivity section from a 2D seismic data, the method of Rosec et al. needs to be applied to each column of this data independently. This deconvolution procedure produces suboptimal results since it does not take into account the spatial dependency between neighboring traces, which stems from the continuous and roughly horizontal structure of the layers of the earth.

Our first goal is to create a modified version of the algorithm of Rosec et al., which performs multichannel deconvolution while taking into account the dependency between neighboring traces. We base our proposed algorithm on the MBG I reflectivity prior model, which takes into account the stratified structure of the 2D reflectivity section. Since the deconvolution problem is blind, the wavelet, noise variance, and the MBG I parameters are unknown, and therefore need to be estimated. We utilize the single-channel blind deconvolution scheme of Rosec et al. for the estimation of these parameters. The obtained parameters are employed by an iterative deconvolution procedure which recovers the columns of the reflectivity in a sequential order, similarly to the method introduced by Idier and Goussard [15]. However, instead of carrying out the estimation using an SMLR-type method, we develop a modified version of the MPM algorithm, which estimates each re-

flectivity column from the corresponding observed trace and the estimate of the preceding reflectivity column.

Our second goal is to improve the performance of the first proposed algorithm, by utilizing estimates of both the preceding and subsequent columns, in the estimation process of each reflectivity column. Thus, in every iteration both the current and subsequent reflectivity columns need to be estimated, since an estimate of the latter is not available from previous iterations. To this end, a further modified version of the MPM algorithm is developed which simultaneously estimates these two columns from the corresponding observed traces and an estimate of the preceding reflectivity column. The estimate of the current reflectivity column, determined from estimates of both its preceding and subsequent neighbors, is kept, while the estimate of the subsequent reflectivity column is discarded, as this column will be reestimated from both its preceding and subsequent neighbors in the next iteration.

1.3 Overview of the Thesis

In this thesis we propose two multichannel blind deconvolution algorithms. Both algorithms are based on the MBG I reflectivity model and iteratively deconvolve the seismic data, while taking into account the spatial dependency between neighboring traces. The first algorithm employs in each iteration a modified version of the MPM algorithm which estimates the current reflectivity column from the corresponding observed trace and the estimate of the preceding reflectivity column. This MPM algorithm estimates the MBRF and amplitude variables corresponding

to the current reflectivity column in two steps. First, it employs a Gibbs sampler to simulate realizations of these variables by iteratively sampling from their conditional distributions, which depend on the estimate of the preceding reflectivity column. Then, a decision step takes place in which the MBRF and amplitude variables are estimated from their realizations. The second algorithm is an extension of the first, which takes into account the dependency between each reflectivity column and both the preceding and subsequent neighbors, in the deconvolution process. It employs in each iteration a further modified MPM algorithm which simultaneously estimates both the current and subsequent reflectivity columns. These columns are determined from the corresponding observed traces and the estimate of the preceding reflectivity column. Again, the estimation is carried out in two steps. First, a Gibbs sampler is employed to simulate realizations of the MBRF and amplitude variables corresponding to the current and subsequent reflectivity columns, by iteratively sampling from their conditional distributions. Then, the MBRF and amplitude variables are determined from their realizations in a decision step. Out of the obtained estimates, only the estimate of the current reflectivity column is kept. The estimate of the subsequent column is discarded, as this column will be determined from estimates of both its preceding and subsequent neighbors in the next iteration. Both multichannel deconvolution algorithms are applied to synthetic and real data, and demonstrate better results compared to those obtained by the single-channel deconvolution method of Rosec el al. The second algorithm which utilizes more information in the estimation process of each reflectivity column is shown to produce better results than the first algorithm.

1.4 Organization

This thesis is organized as follows: In Chapter 2 we describe a single-channel blind deconvolution algorithm proposed by Rosec et al. [10]. We describe the SEM algorithm used for ML parameter estimation. We then describe the MPM algorithm used in the deconvolution procedure. We demonstrate the performance of the algorithm on both real and synthetic data. In Chapter 3, we introduce our first proposed algorithm. We describe the MBG I reflectivity prior model on which the proposed algorithm is based. We then describe a method for the estimation of the parameters of this model, the seismic wavelet and the noise variance. We describe the proposed deconvolution scheme and the modified version of the MPM algorithm utilized by it. We demonstrate the performance of the proposed blind deconvolution method on both real and simulated data and show improvement over the single-channel algorithm presented in Chapter 2. In Chapter 4 we introduce our second proposed algorithm, which is an extension of the algorithm described in Chapter 3. We describe the proposed deconvolution scheme and the further modified MPM algorithm utilized by it. We then present simulation and real data results which demonstrate better performance of the second proposed algorithm compared to the deconvolution algorithms described in Chapters 2 and 3. We summarize the thesis in Chapter 5.

Chapter 2

Single-Channel Blind Deconvolution Using MCMC Methods

2.1 Introduction

The aim of single-channel seismic deconvolution is to recover a 1D reflectivity sequence from a 1D seismic trace, which constitutes a single vertical vector out of the 2D observed seismic data. The 1D trace can be modeled as a convolution between a 1D seismic wavelet and the 1D reflectivity sequence, in the presence of additive noise [23]. When the deconvolution problem is blind, the wavelet is unknown, and both the seismic wavelet and the reflectivity sequence need to be estimated. In this chapter we describe a single-channel blind deconvolution algorithm proposed by Rosec et al. [10]. The reflectivity sequence in the original algorithm is modeled as a

mixture of Gaussian distributions. However, the methods presented next employ a BG model since we assume that the reflectivity sequence appears as a sparse spike train. Rosec et al. proposed two parameter estimation methods. The first method performs maximum likelihood (ML) estimation and use the stochastic expectation maximization (SEM) algorithm [12], [13] to maximize the likelihood criterion. The second method, which estimates the parameters using a Bayesian framework, will not be discussed in our work. Once the missing parameters have been estimated, the next step is the deconvolution itself. The deconvolution problem is "ill-posed" because, in the presence of noise, different reflectivity sequences can lead to similar seismic data. Therefore a priori knowledge upon the reflectivity is introduced in the form of a BG reflectivity assumption, in order to limit the set of acceptable solutions. The deconvolution procedure restores the reflectivity using the suboptimal maximum posterior mode (MPM) method [14], which involves optimization by means of a Gibbs sampler. This chapter is organized as follows: in Section 2.2 we formulate the single-channel blind deconvolution problem. In Section 2.3 we describe the ML parameter estimation procedure, the SEM algorithm and the Gibbs sampler utilized by it. Next, in Section 2.4 we describe the deconvolution procedure and the MPM algorithm. Then in Section 2.5 we present simulated and real data experimental results. Finally we summarize this chapter in Section 2.6.

2.2 Problem Formulation

Single-channel blind seismic deconvolution consists in recovering a 1D reflectivity sequence and a 1D unknown wavelet from a 1D observed seismic

trace. Let $\mathbf{h} = [h(1), ..., h(N_h)]^T$ denote a seismic wavelet of length N_h, and let $\mathbf{r} = [r(1), ..., r(N_r)]^T$ denote a reflectivity sequence of length N_r. Also let $\mathbf{y} = [y(1), ..., y(N_y)]^T$ and $\mathbf{w} = [w(1), ..., w(N_y)]^T$ denote a the seismic trace and a noise vector, respectively, both of length $N_y = N_h + N_r - 1$. Then $\mathbf{y}$ can be modeled as a noisy convolution between the reflectivity sequence $\mathbf{r}$ and the seismic wavelet $\mathbf{h}$

$$y(k) = \sum_{i=1}^{N_h} h(i) r(k-i) + w(k). \tag{2.1}$$

The noise is assumed to be Gaussian with zero mean and variance σ_w^2. The reflectivity $\mathbf{r}$ is represented by a Bernoulli-Gaussian (BG) process, characterized by an underlying state vector $\mathbf{q} = [q(1), ..., q(N_r)]^T$ of independent Bernoulli random variables. Each location variable $q(k)$ is set to one at reflector positions with probability $p(q(k) = 1) = \lambda$, and set to zero otherwise with $p(q(k) = 0) = 1 - \lambda$. The reflectivity sequence $r(k)$ is normally distributed when $q(k) = 1$, with zero mean and variances σ_r^2, and $r(k) = 0$ when $q(k) = 0$, i.e.

$$r(k) \sim \lambda N\left(0, \sigma_r^2\right) + (1 - \lambda)\delta(r(k)). \tag{2.2}$$

Before the deconvolution process can be carried out, the missing parameters $\boldsymbol{\theta} = (\mathbf{h}, \lambda, \sigma_r, \sigma_w)$ need to be estimated from the data $\mathbf{y}$. We next describe the maximum likelihood parameter estimation method.

2.3 Maximum likelihood Parameter Estimation

Maximum likelihood estimation of the parameters $\boldsymbol{\theta}$ is carried out by maximization of the following criterion:

$$\hat{\boldsymbol{\theta}}_{ML} = \underset{\boldsymbol{\theta}}{\operatorname{argmax}} \ln p\left(\mathbf{y}\,|\boldsymbol{\theta}\right). \tag{2.3}$$

Since this is an incomplete data problem, its solution requires the introduction of the missing variables $\mathbf{r}$ and $\mathbf{q}$ and the maximization of the log likelihood of the completed data $L\left(\mathbf{y},\mathbf{r},\mathbf{q}\,|\boldsymbol{\theta}\right) = \ln p\left(\mathbf{y},\mathbf{r},\mathbf{q}\,|\boldsymbol{\theta}\right)$. It is shown in [10] that $L\left(\mathbf{y},\mathbf{r},\mathbf{q}\,|\boldsymbol{\theta}\right)$ is expressed by

$$L\left(\mathbf{y},\mathbf{r},\mathbf{q}\,|\theta\right) = -\frac{\left(\left(\mathbf{y}-\underline{\mathrm{H}}\mathbf{r}\right)^T\left(\mathbf{y}-\underline{\mathrm{H}}\mathbf{r}\right)\right)}{2\sigma_w^2} - \frac{\mathbf{r}^T\underline{\mathrm{Q}}\mathbf{r}}{2\sigma_r^2} - \left(\frac{N_y}{2}\right)\ln\sigma_w^2 + \mathbf{q}^T\mathbf{q}\ln\left(\frac{\lambda}{\sigma_r}\right) \tag{2.4}$$

where $\underline{\mathrm{Q}}$ =diag($\mathbf{q}$) and $\underline{\mathrm{H}}$ and $\underline{\mathrm{R}}$ are the convolution matrices associated with $\mathbf{h}$ and $\mathbf{r}$, respectively. When $\mathbf{r}$ and $\mathbf{q}$ are known the model parameters can be estimated by differentiating $L\left(\mathbf{y},\mathbf{r},\mathbf{q}\,|\theta\right)$. In practice they are unknown, and the SEM algorithm employs a Gibbs sampler to simulate realizations of $\mathbf{r}$ and $\mathbf{q}$ from which it estimates $\boldsymbol{\theta}$. We describe that Gibbs sampler next.

2.3.1 Gibbs sampler

The Gibbs sampler generates samples of $\mathbf{q}$ and $\mathbf{r}$ from the distribution $p\left(\mathbf{r},\mathbf{q}\,|\mathbf{y}\right)$. Instead of sampling directly from the joint distribution $p\left(\mathbf{r},\mathbf{q}\,|\mathbf{y}\right)$, the Gibbs sam-

pler iteratively samples from the distribution $p\left(r\left(k\right),q\left(k\right)\left|\mathbf{y};\mathbf{r}_{-k},\mathbf{q}_{-k}\right.\right)$, where any vector $\mathbf{v}_{-k}$ is defined as $\mathbf{v}_{-k}=\left[v\left(1\right),...,v\left(k-1\right),v\left(k+1\right),...,v\left(N_r\right)\right]$. The distribution $p\left(r\left(k\right),q\left(k\right)\left|\mathbf{y};\mathbf{r}_{-k},\mathbf{q}_{-k}\right.\right)$ can be shown to be [7]:

$$p\left(r\left(k\right),q\left(k\right)\left|\mathbf{y};\mathbf{r}_{-k},\mathbf{q}_{-k}\right.\right)\sim\lambda_k N\left(m_1,V_1\right)+\left(1-\lambda_k\right)\delta\left(r\left(k\right)\right) \tag{2.5}$$

where

$$\lambda_k=p\left(q\left(k\right)=1\left|\mathbf{y};\mathbf{r}_{-k},\mathbf{q}_{-k}\right.\right)=\left[1+\frac{1-\lambda}{\lambda}\sqrt{\frac{\sigma_r^2}{V_1}}\exp\left(-\frac{m_1^2}{2V_1}\right)\right]^{-1} \tag{2.6}$$

and

$V_1=\left(\frac{1}{V_w}+\frac{1}{\sigma_r^2}\right)^{-1}$, $m_1=\frac{V_1}{V_w}m_w$, $V_w=\frac{\sigma_w^2}{E_h}$

$m_w=\frac{1}{E_h}\sum\limits_{i=1}^{N_h}h(i)\left[y\left(k+i-1\right)-\sum\limits_{\substack{j=1\\j\neq i}}^{N_h}h(l)r\left(i+k-j\right)\right]$, $E_h=\sum\limits_{i=1}^{N_h}h^2\left(i\right)$.

Let $B\left(\alpha\right)$ denote a Bernoulli distribution with a parameter α. Then for the simulation of the vectors $\mathbf{r},\mathbf{q}$, the Gibbs sampler follows these steps iteratively:

1. Initialization: choice of $\mathbf{q}^{(0)}$ and $\mathbf{r}^{(0)}$.

2. For $i=1,...,I$

   For $k=1,...,N_r$

   - detection step:
     - compute $\lambda_k=p\left(q\left(k\right)=1\left|\mathbf{y};\mathbf{r}_{-k},\mathbf{q}_{-k}\right.\right)$
     - simulate $q\left(k\right)\sim B\left(\lambda_k\right)$.
   - estimation step:

– simulation of $r^{(i)}(k)$ where $r^{(i)}(k) \sim N(m_1, V_1)$ if $q^{(i)}(k) = 1$ and $r^{(i)}(k) = 0$ if $q^{(i)}(k) = 0$.

2.3.2 SEM algorithm

The SEM algorithm uses realizations of $\mathbf{r}$ and $\mathbf{q}$, simulated by the Gibbs sampler, to estimate the missing parameters $\boldsymbol{\theta}$. It follows these steps iteratively:

1. Initialization: choice of $\mathbf{r}^{(0)}, \mathbf{q}^{(0)}$ and $\boldsymbol{\theta}^{(0)}$;

2. For $i = 1, ...I$:

   - E step: simulate $\mathbf{r}^{(i)}, \mathbf{q}^{(i)}$ using the Gibbs sampler according to $p\left(\mathbf{r}, \mathbf{q} \left| \mathbf{y}, \boldsymbol{\theta}^{(i-1)} \right.\right)$;
   - M step: estimate the parameters

     $\hat{\mathbf{h}}^{(i)} = \left(\underline{\mathrm{R}}^T \underline{\mathrm{R}}\right)^{-1} \underline{\mathrm{R}}^T \mathbf{y}$, $\hat{\sigma}_w^{2\,(i)} = \frac{1}{N_y} \left(\mathbf{y} - \underline{\mathrm{H}}\mathbf{r}\right)^T \left(\mathbf{y} - \underline{\mathrm{H}}\mathbf{r}\right)$

     $\hat{\sigma}_r^{2\,(i)} = \frac{\mathbf{r}^T \mathrm{Q} \mathbf{r}}{\mathbf{q}^T \mathbf{q}}$, $\hat{\lambda}^{(i)} = \frac{\mathbf{q}^T \mathbf{q}}{N_r}$

3. $\hat{\boldsymbol{\theta}} = \frac{1}{I - I_0} \sum_{i=I_0+1}^{I} \boldsymbol{\theta}^{(i)}$

2.4 Deconvolution

Once the parameters $\boldsymbol{\theta}$ are known, the deconvolution problem is reduced to MAP estimation of the hidden variables $\mathbf{r}, \mathbf{q}$ from the observations $\mathbf{y}$

$$(\hat{\mathbf{r}},\ \hat{\mathbf{q}}) = \arg\max_{\mathbf{r},\mathbf{q}} p(\mathbf{r}, \mathbf{q} \,|\mathbf{y}) \tag{2.7}$$

This maximization problem can be solved in two steps using the separation principle [24]:

$$Detection : \hat{\mathbf{q}} = \arg\max_{\mathbf{q}} p\left(\mathbf{q}\,|\mathbf{y}\right) \tag{2.8}$$

$$Estimation : \hat{\mathbf{r}} = \arg\max_{\mathbf{r}} p\left(\mathbf{r}\,|\mathbf{y}, \hat{\mathbf{q}}\right) \tag{2.9}$$

Finding an optimal solution for the detection problem is quite hard because it requires testing all the 2^{N_r} discrete configurations of the vector $\mathbf{q}$, which is very computationally exhaustive and impossible in practice. The solution consists in applying a simpler criterion called the maximum posterior mode (MPM).

2.4.1 MPM algorithm

Instead of maximizing $p\left(\mathbf{r}, \mathbf{q}\,|\mathbf{y}\right)$, the MPM algorithm maximizes the marginal distributions $p\left(r\left(k\right), q\left(k\right)|\mathbf{y}\right)$. Since $p\left(r\left(k\right), q\left(k\right)|\mathbf{y}\right)$ cannot be optimized explicitly, the MPM algorithm uses the Gibbs sampler to simulate realizations of $\mathbf{q}$ and $\mathbf{r}$,which are used to compute the estimates $\hat{\mathbf{q}}$ and $\hat{\mathbf{r}}$. The Gibbs sampler iterates with a learning period $i \leq I_0$ until the simulated Markov chain converges to a stationary distribution. The algorithm further iterates in a steady stage period $I_0 < i \leq I$ in which the generated samples are distributed according to $p\left(\mathbf{r}, \mathbf{q}\,|\mathbf{y}\right)$. The samples $\left(\mathbf{r}^{(i)}, \mathbf{q}^{(i)}\right)$, $I_0 < i \leq I$ created in the steady stage period are first used to estimate each $q\left(k\right)$. Then $r\left(k\right)$ is estimated conditionally to the estimate of $q\left(k\right)$. The MPM algorithm follows theses steps iteratively:

1. For $i = 1, ..., I$ simulate $\left(\mathbf{r}^{(i)}, \mathbf{q}^{(i)}\right)$ using the Gibbs sampler.

2. For $k = 1, ..., N_r$

- detection step:

$$\hat{q}(k) = \begin{cases} 1, & \text{if } \frac{1}{I-I_0} \sum_{i=I_0+1}^{I} q^{(i)}(k) > 0.5 \\ 0, & \text{otherwise} \end{cases}$$

- estimation step:

$$\hat{r}(k) = \begin{cases} \frac{\sum_{i=I_0+1}^{I} q^{(i)}(k) r^{(i)}(k)}{\sum_{i=I_0+1}^{I} q^{(i)}(k)}, & \text{if } \hat{q}(k) = 1 \\ 0, & \text{otherwise} \end{cases}$$

2.5 Results

2.5.1 Synthetic data

We generated a 2D reflectivity section of size 76×100 shown in Fig. 2.1 using the 2D MBG I reflectivity model, described in the next chapter. We then convolved it with a 25 samples long Ricker wavelet and added white Gaussian noise, with signal to noise (SNR) ratios of 0 dB and 5 dB, where the SNR is defined as

$$SNR = 10 \log \left(\frac{\lambda \sigma_r^2 E_h}{\sigma_w^2} \right). \tag{2.10}$$

We created 20 realizations for each SNR and estimated the parameters $\boldsymbol{\theta} = (\mathbf{h}, \lambda, \sigma_r, \sigma_w)$ corresponding to each of the data sets by applying the SEM algorithm to each column of the seismic data and averaging the obtained estimates. Two such realizations with SNRs of 0 dB and 5 dB are shown in Figs. 2.2(a) and (b),

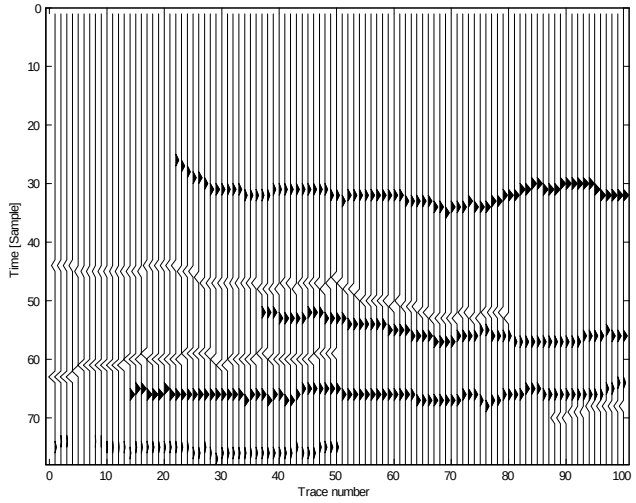

Figure 2.1: Synthetic 2D reflectivity section.

respectively. The true wavelet, along with wavelets estimated for these realizations are shown in Figs. 2.2(c) and (d). The true parameters are shown in Table 2.1, along with the means and standard deviations (in brackets) of the parameters estimated from the realizations with the different SNRs. We define the estimation error obtained for a parameter as the absolute value of the difference between its true value and the mean of its estimates, divided by the true value. Among the estimated parameters, λ was most accurately estimated, with error values of 0.0196 and 0.1303 for SNRs of 0 dB and 5 dB, respectively. On the other hand, the parameters with the largest errors were σ_w with an error of 0.2851 for SNR of 0 dB, and σ_r with an error of 0.1843 for SNR of 5 dB. It can be seen in Table 2.1 and that the accuracy of all the estimated parameters, besides λ, increases with the SNR. It can also be seen in Figs. 2.2(c) and (d) that the accuracy of the estimated wavelet also increases with the SNR.

We next employed the estimated parameters to perform single-channel decon-

Table 2.1: Synthetic 2D example: true and estimated paramters

	True	Estimated (SNR=0 dB)	Estimated (SNR=5 dB)
λ	0.0489	0.0479 (0.0033)	0.0553 (0.0013)
σ_r	1	1.2851 (0.0603)	1.152 (0.0249)
σ_w (SNR=0 dB)	0.2211	0.1742 (0.0035)	-
σ_w (SNR=5 dB)	0.1243	-	0.1014 (0.0012)

volution of each column of the seismic data independently of the others. Note that each reflectivity column estimated by the single-channel deconvolution algorithm had gone through a postprocessing procedure. Whenever this procedure found two or three successive reflectors, or two reflectors separated by one sample, it replaced them by their center of mass. The results obtained for the data sets in Figs. 2.2(a) and (b) are presented in Figs. 2.2(e) and (f), respectively. Both restored reflectivity sections resemble the true reflectivity, but gaps in the boundary layers, misplaced reflectors and scattered false detections can be seen throughout them. It can also be seen that the reflectivity estimate obtained from the trace with the higher SNR is closer to the true reflectivity section.

2.5.2 Real data

We applied the single-channel blind deconvolution scheme to real seismic data shown in Fig. 2.4(a). Similarly to the case of the synthetic data, we estimated the model parameters $\boldsymbol{\theta}$ by applying the SEM algorithm to each column of the 2D real seismic data, and averaging the results. The estimated wavelet is shown in Fig. 2.3 and the estimated parameters can be seen in Table 2.2.

The estimated parameters were next employed to deconvolve the 2D seismic

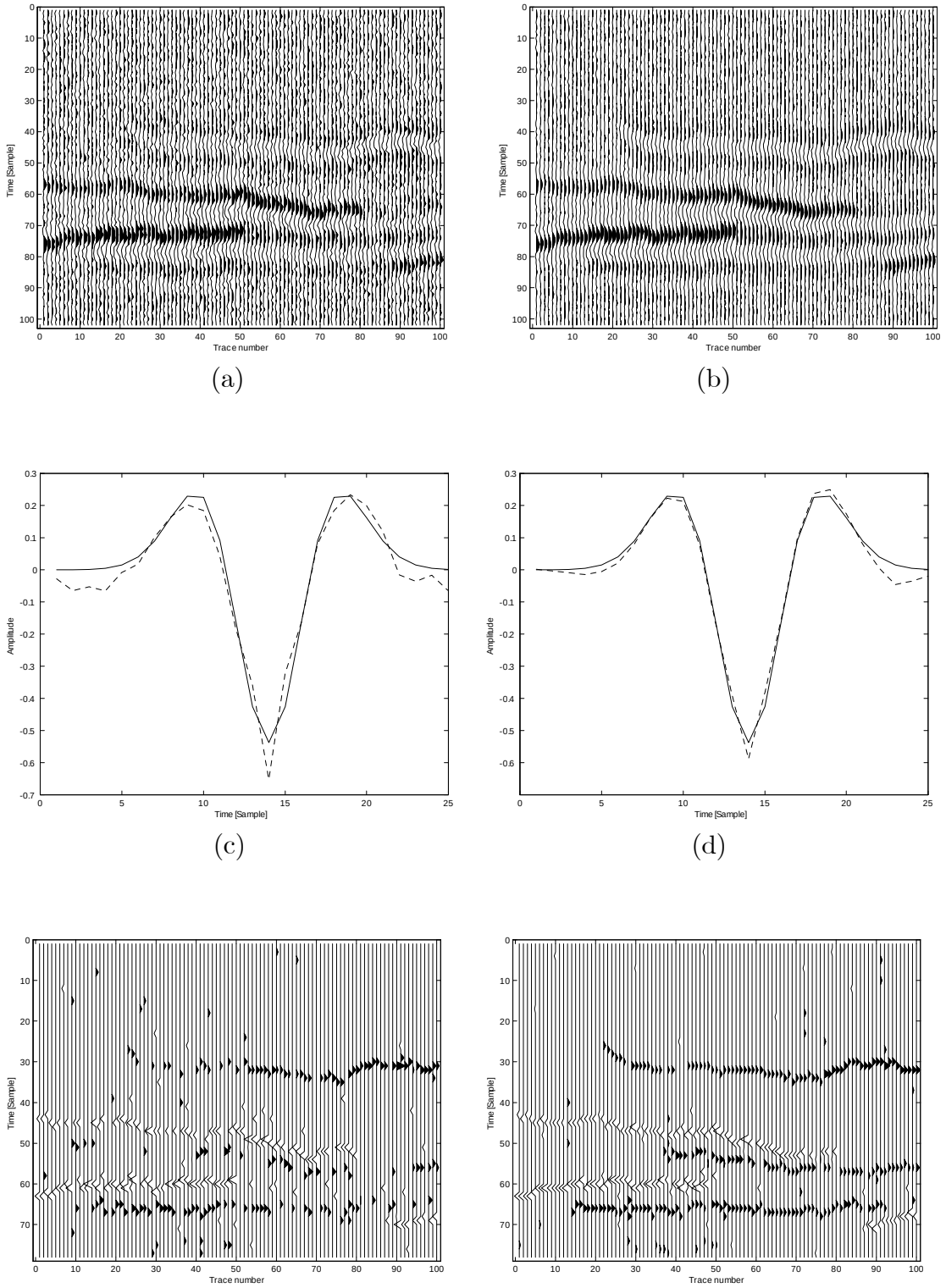

Figure 2.2: Synthetic 2D seismic data single-channel deconvolution results: (a) 2D seismic data (SNR=0 dB). (b) 2D seismic trace (SNR=5 dB). (c) True wavelet (solid) and its estimate (dashed) for SNR=0 dB. (d) True wavelet (solid) and its estimate (dashed) for SNR=5 dB. (e) Estimated 2D reflectivity for SNR=0 dB. (f) Estimated 2D reflectivity for SNR=5 dB.

Table 2.2: Real data example: parameters estimated for the real data

λ	σ_r	σ_w
0.0385	3.9451	0.7008

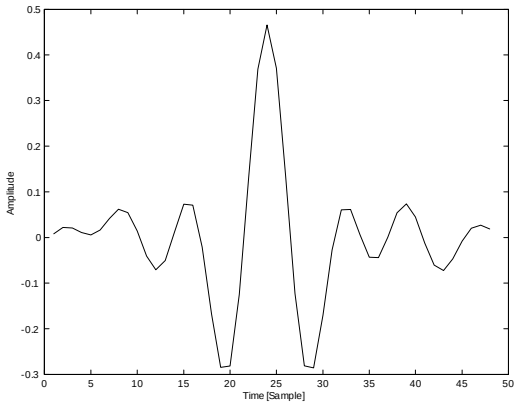

Figure 2.3: Seismic wavelet estimated from real data.

data by applying single-channel deconvolution to each of its columns independently of the others. The obtained estimate of the reflectivity section is shown in Fig. 2.4 (b). The deconvolution process increases the resolution of the seismic image and present a roughly stratified structure. On the other hand, the layer boundaries contain a lot of gaps, only strong reflectors can be easily detected, and a lot of false alarms can be seen throughout the recovered reflectivity section.

2.6 Summary

We have described a single-channel blind deconvolution scheme that was proposed by Rosec et al. This method uses the SEM algorithm to perform ML estimation of the model parameters, and then uses the MPM algorithm to deconvolve the seismic trace. This method was applied to synthetic and real seismic data and was

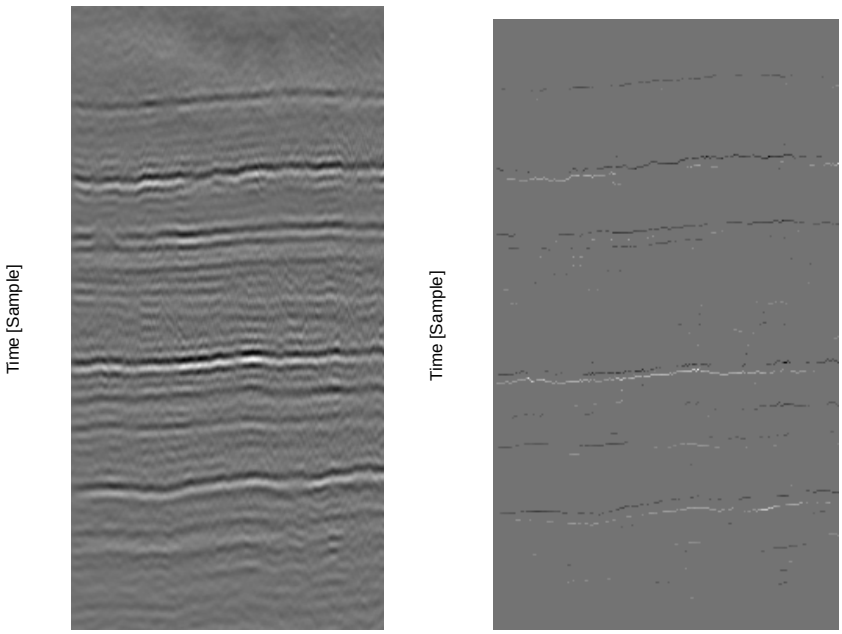

(a) (b)

Figure 2.4: Real data single-channel deconvolution results: (a) Real seismic data. (b) Single-channel deconvolution results.

shown to improve the resolution of the seismic images, achieve better localization of layer boundaries and detect new layers. However, while the recovered reflectivity sections presented a roughly stratified structure, they contained gaps in the layer boundaries and scattered false detections.

The discontinuities in the layer boundaries contained in the estimated reflectivity sections stem from the independent deconvolution of neighboring traces. This problem can be eased by taking into account the dependency between these traces in the deconvolution process, as will be shown in the next chapter.

Chapter 3

Recursive Causal Multichannel Blind Deconvolution

3.1 Introduction

In the previous chapter we have described a single-channel blind deconvolution method proposed by Rosec et al. [10]. We have seen that when this method is applied to 2D simulated and real data, it produces discontinuous reflectivity estimates which contain gaps in the layer boundaries and scattered false detections. The reason for that, is that this 1D restoration method deconvolves each trace independently of all the other traces. As a consequence, the spatial dependency between neighboring traces is ignored and the continuity of the layer boundaries of the reflectivity is not considered in the deconvolution process. In this chapter we propose a modified version of the algorithm of Rosec et al., which performs recursive causal multichannel blind deconvolution. It is based on the MBG I reflectivity

model and iteratively deconvolves the seismic data, while taking into account the dependency between each reflectivity column and its preceding neighbor. In the blind scenario, the MBG I model parameters, the wavelet and the noise variance are unknown, and need to be estimated. We estimate this parameters using the SEM algorithm and from a 2D reflectivity section estimated using the MPM algorithm described in Chapter 2. Once all the missing parameters are known, a modified version of the MPM algorithm estimates in each iteration the current reflectivity column from the corresponding observed trace and an estimate of the preceding reflectivity column. This algorithm is applied to simulated and real data and is shown to produces better results than the ones obtained by the single-channel algorithm of Rosec et al. This chapter is organized as follows: in Section 3.2 we formulate the multichannel blind deconvolution problem. In Section 3.3 we describe the MBG I reflectivity prior model. In Section 3.4 we describe the parameter estimation method. Then in Sections 3.5-3.7 we present the proposed deconvolution scheme, the modified version of the MPM algorithm and the Gibbs sampler employed by it. We present simulated and real data experimental results in Sections 3.8. Finally, we summarize this chapter in Section 3.9.

3.2 Problem Formulation

Multichannel blind seismic deconvolution aims at restoring a 2D reflectivity section and an unknown seismic wavelet from a 2D observed seismic data. The seismic wavelet $\mathbf{h} = [h(1), ..., h(N_h)]^T$ is a 1D vertical vector of length N_h, which is assumed to be invariant in both horizontal and vertical directions. The reflectivity section

$\mathbf{R}$ is a matrix of size $N_r \times J$ and the 2D seismic data $\mathbf{Y}$ is a matrix of size $N_y \times J$, where $N_y = N_h + N_r - 1$. $\mathbf{Y}$ can be modeled as the following noise-corrupted convolution product:

$$\mathbf{Y} = \mathbf{h} * \mathbf{R} + \mathbf{W}. \tag{3.1}$$

where $\mathbf{W}$ is a matrix of size $N_y \times J$ which denotes white Gaussian noise independent of $\mathbf{R}$ with zero mean and variance σ_w^2.

We use the MBG I reflectivity model so that the stratification of the layers of the Earth will be taken into account in the deconvolution process. Since the deconvolution problem is blind, $\mathbf{h}$, σ_w^2 and the MBG I model parameters are unknown, and a method needs to be derived for their estimation. We next describe the MBG I reflectivity model. Then we propose a method for estimating the missing parameters.

3.3 Prior Model

The MBG I reflectivity model [15] is a 2D extension of the 1D BG representation. It is composed of an MBRF, which controls the geometrical characteristics of the reflectivity, and an amplitude field, defined conditionally to the MBRF. The MBRF comprises two kinds of binary variables: location variables and transition variables. The location variables are set in a $N_r \times J$ matrix $\mathbf{Q}$ and indicate the position of layer boundaries. Let $q_{k,j}$ denote the location variable in the in the (k, j) position of $\mathbf{Q}$. Then $q_{k,j}$ is set to one if a reflector exists in the (k, j) position of $\mathbf{R}$, and is set to zero otherwise. The transition variables are set in three $N_r \times J - 1$ matrices

$\mathbf{T}^{/}$, $\mathbf{T}^{-}$ and $\mathbf{T}^{\backslash}$ and determine whether adjacent location variables belong to the same layer boundary or not. Let $t^{/}_{k,j}$, $t^{-}_{k,j}$, $t^{\backslash}_{k,j}$ denote the transition variables in the (k,j) positions of $\mathbf{T}^{/}$, $\mathbf{T}^{-}$ and $\mathbf{T}^{\backslash}$, respectively. Then $t^{/}_{k,j}$ is set to one if $q_{k,j}$ and $q_{k-1,j+1}$ belong to the same layer boundary and to zero otherwise. Similarly $t^{-}_{k,j}$ and $t^{\backslash}_{k,j}$ are set to one if $q_{k,j}$ belongs to the same layer boundary as $q_{k,j+1}$ and $q_{k+1,j+1}$, respectively, and to zero otherwise. Therefore, $t^{/}_{k,j}$, $t^{-}_{k,j}$ and $t^{\backslash}_{k,j}$ determine whether layer boundaries whose orientation is diagonally ascending, horizontal, and diagonally descending, respectively, exist in the (k,j) position of $\mathbf{Q}$. Figure. 3.1(a) shows a representation of layer boundaries and their orientation in several locations using location and transitions variables. Gray squares denote the presence of a layer boundary and arrows facing upward, rightward and downward correspond to positions in which $t^{/}_{k,j}, t^{-}_{k,j}$ and $t^{\backslash}_{k,j}$, respectively, are set to one. Figure. 3.1(b) shows the location variable $q_{k,j}$, all the location variables which may be on the same boundary with it, and the transition variables between them.

The MBRF has the following properties:

1. Separability property: $p\left(t^{/}_{k,j}, t^{-}_{k,j}, t^{\backslash}_{k,j}\right) = p\left(t^{/}_{k,j}\right) p\left(t^{-}_{k,j}\right) p\left(t^{\backslash}_{k,j}\right)$.

2. The jth columns of $\mathbf{Q}$, $\mathbf{T}^{/}$, $\mathbf{T}^{-}$ and $\mathbf{T}^{\backslash}$, denoted $\mathbf{q}_j$, $\mathbf{t}^{/}_j$, $\mathbf{t}^{-}_j$ and $\mathbf{t}^{\backslash}_j$, respectively, are white and Bernoulli distributed marginally from the rest of the field.

3. The characteristic parameters of the Bernoulli distributions are given by: $\lambda = p\left(q_{k,j} = 1\right)$, $\mu^{/} = p\left(t^{/}_{k,j} = 1\right)$, $\mu^{-} = p\left(t^{-}_{k,j} = 1\right)$, $\mu^{\backslash} = p\left(t^{\backslash}_{k,j} = 1\right)$.

4. Horizontal symmetry:
$p\left(q_{k,j}, t^{/}_{k,j}, t^{-}_{k,j}, t^{\backslash}_{k,j}\right) = p\left(q_{k,j}, t^{/}_{k+1,j-1}, t^{-}_{k,j-1}, t^{\backslash}_{k-1,j+1}\right)$.

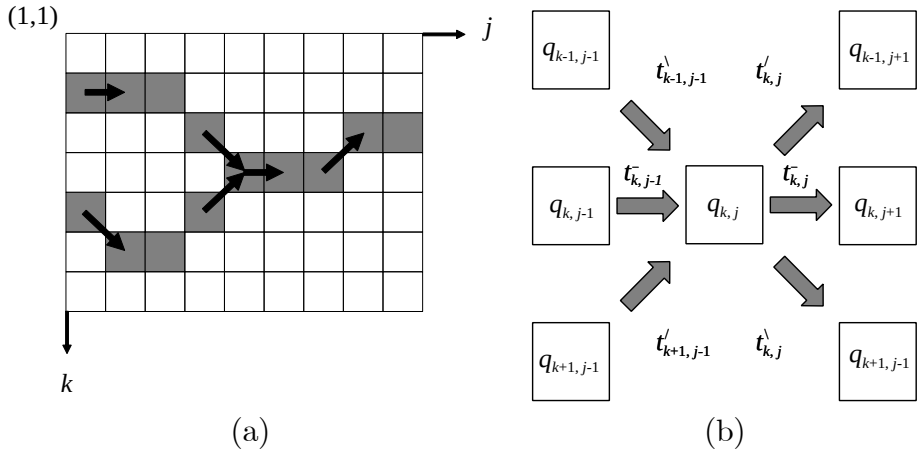

(a) (b)

Figure 3.1: Location and transition variables: (a) Layer boundaries representaion. (b) Location variable $q_{k,j}$ and other location and transition varibles affected by it

5. Isolated transition variables cannot be set to one:

$$p\left(t^{/}_{k,j}=0, t^{-}_{k,j}=0, t^{\backslash}_{k,j}=0\,|q_{k,j}=0\right)=1.$$

6. Discontinuities along layer boundaries are possible:

$$p\left(q_{k,j}=1\,\middle|\,t^{/}_{k+1,j-1}=0, t^{-}_{k,j-1}=0, t^{\backslash}_{k-1,j-1}=0\right)=\varepsilon.$$

7. λ is related to $\left\{\mu^{/},\mu^{-},\mu^{\backslash},\varepsilon\right\}$ according to:

$$\lambda=1-\left(1-\mu^{/}\right)\left(1-\mu^{-}\right)\left(1-\mu^{\backslash}\right)\left(1-\varepsilon\right).$$

We now turn to the amplitude field $\mathbf{R}$. The MBG I model assumes that the amplitudes of the reflectors are independent in the vertical direction and that marginally from the rest of the field, the amplitude of each reflector is normally distributed with zero mean and variance equal to σ_r^2. The conditional probability of the amplitude field of the reflectivity $p\left(\mathbf{R}\,\middle|\,\mathbf{T}^{/},\ \mathbf{T}^{-},\ \mathbf{T}^{\backslash},\ \mathbf{Q}\right)$ is assumed to

have a first-order Markov chain structure, and each reflector is assumed to be correlated only with reflectors located on the same boundary. Let $\mathbf{r}_j$ denotes the jth column of $\mathbf{R}$, and let $r_{k,j}$ denote the kth reflector in $\mathbf{r}_j$. Then the correlation between $r_{k,j}$ and reflectors in previous columns depends on the local geometry of the layers and is described through $p\left(r_{k,j}\left|q_{k,j},\mathbf{t}^{/}_{j-1},\mathbf{t}^{-}_{j-1},\mathbf{t}^{\backslash}_{j-1},\mathbf{r}_{j-1}\right.\right)$. Let $t^{/}_{k+1,j-1}$ (respectively, $t^{-}_{k,j-1}$, $t^{\backslash}_{k+1,j-1}$) be set to one, then we will further refer to the reflector $r_{k,j}$ as a successor of $r_{k+1,j-1}$ (respectively $r_{k,j-1}$, $r_{k-1,j-1}$) and symmetrically $r_{k+1,j-1}$ (respectively $r_{k,j-1}$, $r_{k-1,j-1}$) will be referred to as a predecessor of $r_{k,j}$. The conditional probabilities $p\left(r_{k,j}\left|q_{k,j},\mathbf{t}^{/}_{j-1},\mathbf{t}^{-}_{j-1},\mathbf{t}^{\backslash}_{j-1},\mathbf{r}_{j-1}\right.\right)$ can be separated into four cases which depend on the existence and uniqueness of successors and predecessors:

1. If $q_{k,j}=0$ then there is no reflector at position (k,j), and $r_{k,j}=0$.

2. If $q_{k,j}=1$, and if $r_{k,j}$ is the unique successor of a unique predecessor $r_{k+dk,j-1}\,(-1\leq dk\leq 1)$, then $r_{k,j}$ is sampled from a first-order autoregressive (AR) process, conditionally to $r_{k+dk,j-1}$. This case corresponds to interactions along a single layer boundary. Let $a\in[0,1]$ control the degree of correlation between reflector amplitudes along the same boundary and let $w_r\sim N\left[0,\left(1-a^2\right)\sigma_r^2\right]$, then the AR process is defined by

$$r_{k,j}=ar_{k+dk,j-1}+w_r. \tag{3.2}$$

3. If $q_{k,j}=1$ and if $r_{k,j}$ has no predecessor, then $r_{k,j}$ is sampled from the basic Gaussian distribution $N\left(0,\sigma_r^2\right)$.

4. If $q_{k,j} = 1$ and if $r_{k,j}$ has more than one predecessor, or symmetrically when $r_{k,j}$ is not a unique predecessor, then $r_{k,j}$ is sampled from the basic Gaussian distribution $N(0, \sigma_r^2)$.

Before the deconvolution can be performed, the parameters of this 2D reflectivity model need to be estimated from the data, along with the seismic wavelet and the noise variance. We next describe the parameter estimation method.

3.4 Parameter estimation

Our goal is to estimate the parameters $\boldsymbol{\theta} = (\mathbf{h}, \lambda, \sigma_r, \sigma_w)$ and the MBG I parameters $\boldsymbol{\theta}_{MBG} = \left(a, \mu^{/}, \mu^{-}, \mu^{\backslash}, \varepsilon\right)$ from the observed trace $\mathbf{Y}$. We estimate the parameters $\boldsymbol{\theta}$ using the SEM algorithm, in the same way they were estimated in Chapter 2. Let $\mathbf{y}_j$ denote the jth trace of the seismic data. Then we apply the SEM algorithm to each of the traces $\mathbf{y}_j$ and obtain from each trace an estimate $\hat{\boldsymbol{\theta}}_j$. Since the parameters $\boldsymbol{\theta}$ are assumed common to all the seismic traces, the final estimate $\hat{\boldsymbol{\theta}} = \left(\hat{\mathbf{h}}, \hat{\lambda}, \hat{\sigma}_r, \hat{\sigma}_w\right)$ is obtained by averaging the estimates $\hat{\boldsymbol{\theta}}_j$. We now proceed to estimate the parameters $\boldsymbol{\theta}_{MBG}$. We employ the parameters $\hat{\boldsymbol{\theta}}$ to deconvolve each of the traces $\mathbf{y}_j$ using the MPM algorithm described in Chapter 2. We then remove all the isolated reflectors from the obtained reflectivity estimate and term the result $\hat{\mathbf{R}}^c_{TBT}$. Now, let $I^{/}$, I^{-} and $I^{\backslash}$ denote the number of positions in $\hat{\mathbf{R}}^c_{TBT}$ in which the orientation of the layer boundaries is ascending, horizontal

and descending, respectively. Then we propose the following estimators:

$$\begin{aligned}\hat{\mu}^{/} &= \frac{I^{/}}{(J-1)\,N_r} \\ \hat{\mu}^{-} &= \frac{I^{-}}{(J-1)\,N_r} \\ \hat{\mu}^{\backslash} &= \frac{I^{\backslash}}{(J-1)\,N_r} \\ \hat{\varepsilon} &= 1-(1-\hat{\lambda})/(1-\hat{\mu}^{/})/(1-\hat{\mu}^{-})/(1-\hat{\mu}^{\backslash}).\end{aligned} \tag{3.3}$$

We recall that reflectors along a single layer boundary are sampled from a first-order AR process whose parameter is a. Therefore a can be estimated by calculating the first-order Yule Walker equations for each layer boundary, and averaging the results. Let $\mathbf{I}_l$ be the number of layer boundaries in $\hat{\mathbf{R}}^{c}_{TBT}$, and let $\mathbf{l}_m = [l_m(1), ..., l_m(L_m)]^T$ be the reflectors of the mth boundary arranged in a vector of length L_m. Then:

$$\hat{a}_{YW} = \frac{1}{I_l}\sum_{m=1}^{I_l}\left[\frac{\sum_{k=1}^{L_m-1} l_m(k+1)\,l_m(k)}{\sum_{k=1}^{L_m-1} l_m^2(k+1)}\right]. \tag{3.4}$$

The obtained estimate $\hat{a}_{YW}$ is usually very close to the true value of a. However, simulation results (not reported her) showed that better deconvolution results are obtained by a heuristic estimator, which calculates the average attenuation ratio between neighboring reflectors. In the sequel the following estimator is used:

$$\hat{a} = \frac{1}{I_l}\sum_{m=1}^{I_l}\left[\frac{1}{L_m-1}\sum_{k=1}^{L_m-1}\min\left(\frac{l_m(k+1)}{l_m(k)}, \frac{l_m(k)}{l_m(k+1)}\right)\right]. \tag{3.5}$$

Once all the missing parameters are known, multichannel deconvolution can be performed. We next describe the first proposed multichannel deconvolution procedure.

3.5 Deconvolution Scheme

The MAP estimator of the matrices $\left\{\mathbf{T}^{/}, \mathbf{T}^{-}, \mathbf{T}^{\backslash}, \mathbf{Q}\right\}$, comprising the MBRF, and the amplitude field $\mathbf{R}$ is:

$$\left(\hat{\mathbf{T}}^{/}, \hat{\mathbf{T}}^{-}, \hat{\mathbf{T}}^{\backslash}, \hat{\mathbf{Q}}, \hat{\mathbf{R}}\right) = \underset{\mathbf{T}^{/}, \mathbf{T}^{-}, \mathbf{T}^{\backslash}, \mathbf{Q}, \mathbf{R}}{\operatorname{argmax}} p\left(\mathbf{T}^{/}, \mathbf{T}^{-}, \mathbf{T}^{\backslash}, \mathbf{Q}, \mathbf{R} \,|\mathbf{Y}\right). \tag{3.6}$$

Computing the exact MAP solution is a very hard problem, even when the efficient Viterbi algorithm is used, because of the large dimension of the state-space of $\left\{\mathbf{T}^{/}, \mathbf{T}^{-}, \mathbf{T}^{\backslash}, \mathbf{Q}\right\}$. However, Idier and Goussard [15] showed that the a posteriori likelihood $p\left(\mathbf{T}^{/}, \mathbf{T}^{-}, \mathbf{T}^{\backslash}, \mathbf{Q}, \mathbf{R} \,|\mathbf{Y}\right)$ can be expressed as:

$$p\left(\mathbf{T}^{/}, \mathbf{T}^{-}, \mathbf{T}^{\backslash}, \mathbf{Q}, \mathbf{R} \,|\mathbf{Y}\right) \propto p\left(\mathbf{q}_1, \mathbf{r}_1, \mathbf{y}_1\right) \prod_{j=2}^{J} p\left(\mathbf{t}_{j-1}, \mathbf{q}_j, \mathbf{r}_j, \mathbf{y}_j \,|\mathbf{q}_{j-1}, \mathbf{r}_{j-1}\right) \tag{3.7}$$

This formula led them to propose the following suboptimal recursive causal maximization procedure:

$$(1)\ \text{First column:}\ \ (\hat{\mathbf{r}}_1, \hat{\mathbf{q}}_1) = \underset{\mathbf{r}_1, \mathbf{q}_1}{\operatorname{argmax}}\, p\left(\mathbf{q}_1, \mathbf{r}_1, \mathbf{y}_1\right) \tag{3.8}$$

$$(2)\ j \in [2, J] : \left(\hat{\mathbf{r}}_j, \hat{\mathbf{q}}_j, \hat{\mathbf{t}}^{/}_{j-1}, \hat{\mathbf{t}}^{-}_{j-1}, \hat{\mathbf{t}}^{\backslash}_{j-1}\right)$$

$$= \underset{\mathbf{r}_j, \mathbf{q}_j, \mathbf{t}^{/}_{j-1}, \mathbf{t}^{-}_{j-1}, \mathbf{t}^{\backslash}_{j-1}}{\operatorname{argmax}} p\left(\mathbf{r}_j, \mathbf{q}_j, \mathbf{t}^{/}_{j-1}, \mathbf{t}^{-}_{j-1}, \mathbf{t}^{\backslash}_{j-1}, \mathbf{y}_j \,|\hat{\mathbf{q}}_{j-1}, \hat{\mathbf{r}}_{j-1}\right) \tag{3.9}$$

where SMLR-type algorithms were used for the optimization of the partial criteria (3.8) and (3.9). Here we use a similar iterative maximization procedure, which employs MCMC methods for the optimization of its partial criteria. We first rewrite (3.8) and (3.9) as:

$$(1)\ \text{First column:}\ \ (\hat{\mathbf{r}}_1, \hat{\mathbf{q}}_1) = \underset{\mathbf{r}_1, \mathbf{q}_1}{\operatorname{argmax}}\, p\left(\mathbf{r}_1, \mathbf{q}_1 \,|\mathbf{y}_1\right) \tag{3.10}$$

$$(2)\ j \in [2, J] : \left(\hat{\mathbf{r}}_j, \hat{\mathbf{q}}_j, \hat{\mathbf{t}}^{/}_{j-1}, \hat{\mathbf{t}}^{-}_{j-1}, \hat{\mathbf{t}}^{\backslash}_{j-1}\right)$$

$$= \underset{\mathbf{r}_j, \mathbf{q}_j, \mathbf{t}^{/}_{j-1}, \mathbf{t}^{-}_{j-1}, \mathbf{t}^{\backslash}_{j-1}}{\operatorname{argmax}} p\left(\mathbf{r}_j, \mathbf{q}_j, \mathbf{t}^{/}_{j-1}, \mathbf{t}^{-}_{j-1}, \mathbf{t}^{\backslash}_{j-1} \,|\mathbf{y}_j, \hat{\mathbf{r}}_{j-1}, \hat{\mathbf{q}}_{j-1}\right) \tag{3.11}$$

In the first iteration $\mathbf{r}_1$ and $\mathbf{q}_1$ are determined from the first observed trace $\mathbf{y}_1$. In each following iteration, the reflectivity column $\mathbf{r}_j$, $j \in [2, J]$ and corresponding hidden binary vectors $\mathbf{t}^{/}_{j-1}, \mathbf{t}^{-}_{j-1}, \mathbf{t}^{\backslash}_{j-1}, \mathbf{q}_j$ are determined from the current observed trace $\mathbf{y}_j$ and the estimates of $\mathbf{r}_{j-1}$ and $\mathbf{q}_{j-1}$, obtained in the previous iteration. This maximization procedure is suboptimal since for $j > 1$ each partial criterion is maximized only with respect to $\mathbf{r}_j, \mathbf{q}_j, \mathbf{t}^{/}_{j-1}, \mathbf{t}^{-}_{j-1}, \mathbf{t}^{\backslash}_{j-1}$ and all the previously estimated quantities remain unchanged. Also, the determination of $\mathbf{r}_j$ is based

on observations only up to $\mathbf{y}_j$ and subsequent columns of the observed data, which are very informative about $\mathbf{r}_j$, are not taken into account in its estimation. On the other hand, this method is much simpler than global maximization of $p\left(\mathbf{T}^{/}, \mathbf{T}^{-}, \mathbf{T}^{\backslash}, \mathbf{Q}, \mathbf{R} \,|\mathbf{Y}\right)$, and does take into account the dependency between neighboring reflectivity columns, unlike single-channel deconvolution methods.

The first partial criterion can be optimized using the MPM algorithm described in Chapter 2. Finding an optimal solution for the maximization problem (3.11) is a very hard, since it requires examination of all the possible configurations of $\mathbf{q}_j, \mathbf{t}^{/}_{j-1}, \mathbf{t}^{-}_{j-1}, \mathbf{t}^{\backslash}_{j-1}$, whose number ranges from 2^{N_r} to 8^{N_r}. Therefore, we apply instead a modified version of the MPM algorithm. This algorithm estimates the vectors $\mathbf{r}_j, \mathbf{q}_j, \mathbf{t}^{/}_{j-1}, \mathbf{t}^{-}_{j-1}, \mathbf{t}^{\backslash}_{j-1}$ from realizations simulated by a Gibbs sampler, described next.

3.6 Gibbs Sampler

The Gibbs sampler generates samples of $\mathbf{r}_j, \mathbf{q}_j, \mathbf{t}^{/}_{j-1}, \mathbf{t}^{-}_{j-1}, \mathbf{t}^{\backslash}_{j-1}$ from the joint distribution $p\left(\mathbf{r}_j, \mathbf{q}_j, \mathbf{t}^{/}_{j-1}, \mathbf{t}^{-}_{j-1}, \mathbf{t}^{\backslash}_{j-1} \,|\mathbf{y}_j, \hat{\mathbf{r}}_{j-1}, \hat{\mathbf{q}}_{j-1}\right)$. Instead of sampling directly from this joint distribution, the Gibbs sampler iteratively samples from the conditional distributions:

1. $p\left(t^{/}_{k,j-1} \left| \mathbf{r}_j, \mathbf{q}_j, \mathbf{t}^{/}_{-k,j-1}, \mathbf{t}^{-}_{j-1}, \mathbf{t}^{\backslash}_{j-1}, \hat{\mathbf{r}}_{j-1}, \hat{\mathbf{q}}_{j-1}\right.\right) \sim B\left(\mu^{/}_{k,j-1}\right)$
2. $p\left(t^{-}_{k,j-1} \left| \mathbf{r}_j, \mathbf{q}_j, \mathbf{t}^{/}_{j-1}, \mathbf{t}^{-}_{-k,j-1}, \mathbf{t}^{\backslash}_{j-1}, \hat{\mathbf{r}}_{j-1}, \hat{\mathbf{q}}_{j-1}\right.\right) \sim B\left(\mu^{-}_{k,j-1}\right)$
3. $p\left(t^{\backslash}_{k,j-1} \left| \mathbf{r}_j, \mathbf{q}_j, \mathbf{t}^{/}_{,j-1}, \mathbf{t}^{-}_{j-1}, \mathbf{t}^{\backslash}_{-k,j-1}, \hat{\mathbf{r}}_{j-1}, \hat{\mathbf{q}}_{j-1}\right.\right) \sim B\left(\mu^{\backslash}_{k,j-1}\right)$

4. $p\left(r_{k,j}, q_{k,j} \left| \mathbf{y}_j, \mathbf{r}_{-k,j}, \mathbf{q}_{-k,j}, \mathbf{t}^{/}_{j-1}, \mathbf{t}^{-}_{j-1}, \mathbf{t}^{\backslash}_{j-1}, \hat{\mathbf{r}}_{j-1} \right.\right) \sim \lambda^b_{k,j} N\left(m^b_{k,j}, V^b_{k,j}\right) + \left(1-\lambda^b_{k,j}\right)\delta\left(r_{k,j}\right)$

where the derivation of $\mu^{/}_{k,j-1}$, $\mu^{-}_{k,j-1}$, $\mu^{\backslash}_{k,j-1}$, $\lambda^b_{k,j}$, $m^b_{k,j}$ and $V^b_{k,j}$ can be found in Sections A.1 and A.2 of the appendix.

For the simulation of the vectors $\mathbf{r}_j$, $\mathbf{q}_j$, $\mathbf{t}^{/}_{j-1}, \mathbf{t}^{-}_{j-1}$ and $\mathbf{t}^{\backslash}_{j-1}$, the Gibbs sampler follows these steps iteratively:

1. Initialization: choice of $\mathbf{q}^{(0)}_j$, $\mathbf{r}^{(0)}_j, \mathbf{t}^{/\,(0)}_{j-1}, \mathbf{t}^{-\,(0)}_{j-1}$ and $\mathbf{t}^{\backslash\,(0)}_{j-1}$.

2. For $i = 1, ..., I$

   For $k = 1, ..., N_r$

   - detection step:
     - compute $\mu^{/}_{k,j-1}$ using (A.18) and simulate $t^{/\,(i)}_{k,j-1} \sim B\left(\mu^{/}_{k,j-1}\right)$
     - compute $\mu^{-}_{k,j-1}$ using (A.24) and simulate $t^{-\,(i)}_{k,j-1} \sim B\left(\mu^{-}_{k,j-1}\right)$
     - compute $\mu^{\backslash}_{k,j-1}$ using (A.30) and simulate $t^{\backslash\,(i)}_{k,j-1} \sim B\left(\mu^{\backslash}_{k,j-1}\right)$
     - compute $\lambda^b_{k,j}$ using (A.8) and simulate $q^{(i)}_{k,j} \sim B\left(\lambda^b_{k,j}\right)$
   - estimation step:
     - simulate $r^{(i)}_{k,j}$ where $r^{(i)}_{k,j} \sim N\left(m^b_{k,j}, V^b_{k,j}\right)$ if $q^{(i)}_{k,j} = 1$ and $r^{(i)}_{k,j} = 0$ if $q^{(i)}_{k,j} = 0$.

3.7 MPM algorithm

We estimate each column $\mathbf{r}_j$, $1 < j \leq J$ using a modified version of the MPM algorithm. This algorithm employs the Gibbs sampler de-

scribed above to generate realizations of $\mathbf{r}_j, \mathbf{q}_j, \mathbf{t}^{/}_{j-1}, \mathbf{t}^{-}_{j-1}$ and $\mathbf{t}^{\backslash}_{j-1}$ drawn from $p\left(\mathbf{r}_j, \mathbf{q}_j, \mathbf{t}^{/}_{j-1}, \mathbf{t}^{-}_{j-1}, \mathbf{t}^{\backslash}_{j-1} \,|\mathbf{y}_j, \hat{\mathbf{r}}_{j-1}, \hat{\mathbf{q}}_{j-1}\right)$. The Gibbs sampler performs I_0 iterations until it reaches a steady state period. The samples $\left(\mathbf{r}_j^{(i)}, \mathbf{q}_j^{(i)}, \mathbf{t}^{/\,(i)}_{j-1}, \mathbf{t}^{-\,(i)}_{j-1}, \mathbf{t}^{\backslash\,(i)}_{j-1}\right)$ produced in the following iterations $I_0 < i \leq I$ are used to first estimate each of $q_{k,j}$, $t^{/}_{k,j-1}$, $t^{-}_{k,j-1}$, $t^{\backslash}_{k,j-1}$, and then determine $r_{k,j}$ conditionally to the estimate of $q_{k,j}$. The modified MPM algorithm follows these steps iteratively:

1. For $i = 1, ..., I$ simulate $\left(\mathbf{r}_j^{(i)}, \mathbf{q}_j^{(i)}, \mathbf{t}^{/\,(i)}_{j-1}, \mathbf{t}^{-\,(i)}_{j-1}, \mathbf{t}^{\backslash\,(i)}_{j-1}\right)$ using the Gibbs sampler.

2. For $k = 1, ..., N_r$

   - detection step:

$$\hat{t}^{/}_{k,j-1} = \begin{cases} 1, & \text{if } \frac{1}{I-I_0} \sum_{i=I_0+1}^{I} t^{/\,(i)}_{k,j-1} > 0.5 \\ 0, & \text{otherwise} \end{cases},$$

$$\hat{t}^{-}_{k,j-1} = \begin{cases} 1, & \text{if } \frac{1}{I-I_0} \sum_{i=I_0+1}^{I} t^{-\,(i)}_{k,j-1} > 0.5 \\ 0, & \text{otherwise} \end{cases},$$

$$\hat{t}^{\backslash}_{k,j-1} = \begin{cases} 1, & \text{if } \frac{1}{I-I_0} \sum_{i=I_0+1}^{I} t^{\backslash\,(i)}_{k,j-1} > 0.5 \\ 0, & \text{otherwise} \end{cases},$$

$$\hat{q}_{k,j} = \begin{cases} 1, & \text{if } \frac{1}{I-I_0} \sum_{i=I_0+1}^{I} q^{(i)}_{k,j} > 0.5 \\ 0, & \text{otherwise} \end{cases}$$

   - estimation step

$$\hat{r}_{k,j} = \begin{cases} \frac{\sum_{i=I_0+1}^{I} q^{(i)}_{k,j} r^{(i)}_{k,j}}{\sum_{i=I_0+1}^{I} q^{(i)}_{k,j}(k)}, & \text{if } \hat{q}_{k,j} = 1 \\ 0, & \text{otherwise} \end{cases}$$

3.8 Experimental results

3.8.1 Synthetic data:

We employed the proposed parameter estimation method to find the missing parameters corresponding to each of the data sets synthesized in Section 2.5.1. The true parameters are shown in Table 3.1, along with the means and standard deviations (in brackets) of the parameters estimated from the realizations with the different SNRs. Note that the estimates obtained here for the parameters $\boldsymbol{\theta} = (\mathbf{h}, \lambda, \sigma_r, \sigma_w)$ are identical to the ones obtained in the previous chapter, since in both cases these parameters were estimated exactly in the same manner. The true and estimated wavelets obtained for the data sets with SNRs of 0 dB and 5 dB, shown in Figs. 2.2(a) and (b), are redepicted in Figs. 3.3(a) and (b),respectively.

Table 3.1: Synthetic 2D example: true and estimated paramters

	True	Estimated (SNR=0 dB)	Estimated (SNR=5 dB)
λ	0.0489	0.0479 (0.0033)	0.0553 (0.0013)
σ_r	1	1.2851 (0.0603)	1.152 (0.0249
σ_w (SNR=0 dB)	0.2211	0.1742 (0.0035)	-
σ_w (SNR=5 dB)	0.1243	-	0.1014 (0.0012)
a	0.999	0.7752 (0.0202)	0.7899 (0.0152)
$\mu^{/}$	0.008	0.0058 (0.0007)	0.0076 (0.0008)
μ^{-}	0.033	0.01 (0.0011)	0.0228 (0.0017)
$\mu^{\backslash}$	0.008	0.0061 (0.0008)	0.0086 (0.0007)
ε	0.0005	0.0266 (0.0034)	0.0174 (0.0019)

We define the estimation error obtained for a parameter as the absolute value of the difference between its true value and the mean of its estimates, divided by the true value. Among the estimated parameters, the parameter ε has the largest error, with error values of 52.2791 and 33.8524 for SNRs of 0 dB and 5 dB, respectively. On the other hand, the parameters most accurately estimated

were: λ for SNR of 0 dB, with an error of 0.0196, and $\mu^{/}$ for SNR of 5 dB, with an error of 0.0522. Also, the accuracy of all the estimated parameters, besides λ, improves as the SNR increases. The largest improvement is obtained for ε where the estimation error decreases from 52.2791 to 33.8524, and the smallest improvement is obtained for a, where the estimation error decreases from 0.2240 to 0.2093. As already mentioned above, it can be seen in Figs. 3.3(a) and (b) that the accuracy of the estimated wavelet also increases with the SNR.

The estimated parameters were employed by the deconvolution scheme of the proposed multichannel algorithm, where each estimated reflectivity column had gone through the postprocessing procedure described in the Section 2.5.1. We will hereafter refer to the first proposed algorithm as Multi-channel I (MC I). We also used the reflectivity sections recovered in the previous chapter by single-channel deconvolution for comparison reasons. The true reflectivity section is redepicted in Fig. 3.2. The results of single-channel deconvolution and the MC I algorithm, obtained for the data sets with SNRs of 0 dB and 5 dB depicted in Figs. 2.2(a) and (b), are shown in Fig. 3.3. Visual comparison between these results shows improved performance of the MC I algorithm over the performance of the single-channel deconvolution algorithm. For both SNR levels the estimates of MC I are more continuous, contain less false detections and are generally closer to the true reflectivity than the single-channel deconvolution results.

In order to quantify the performances of the MC I and single-channel algorithms and compare them to each other, we used the four loss functions suggested by Kaaresen in [25]. Let $\mathbf{r}$ be a 1D reflectivity sequence and $\hat{\mathbf{r}}$ be its estimate, and

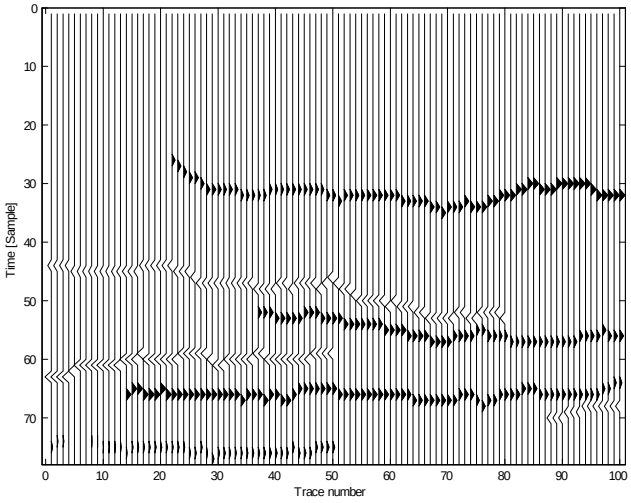

Figure 3.2: Synthetic 2D reflectivity section

let $\|\cdot\|_1$ and $\|\cdot\|_2$ be the L_1 and L_2 norm, respectively. Also, let $N^{miss} = \#\{n : \hat{r}(n) = 0,\, r(n) \neq 0\}$ and $N^{false} = \#\{n : \hat{r}(n) \neq 0,\, r(n) = 0\}$ denote the number of missed and false detections in $\hat{\mathbf{r}}$, respectively. Then the loss functions are:

$$\begin{aligned} L^{miss+false} &= \|\hat{\mathbf{r}} - \mathbf{r}\|_1 + N^{miss} + N^{false} \\ L^{miss} &= \|\hat{\mathbf{r}} - \mathbf{r}\|_1 + N^{miss} \\ L^{false} &= \|\hat{\mathbf{r}} - \mathbf{r}\|_1 + N^{false} \\ L^{SSQ} &= \|\hat{\mathbf{r}} - \mathbf{r}\|_2 . \end{aligned} \tag{3.12}$$

Kaaresen also suggested to make the loss functions more realistic, by regarding estimated reflectors that were close to their true positions as partially correct. Therefore we added three loss functions which treated reflectors in $\hat{\mathbf{r}}$ with an offset of one sample from their true location as if they were set in their true locations,

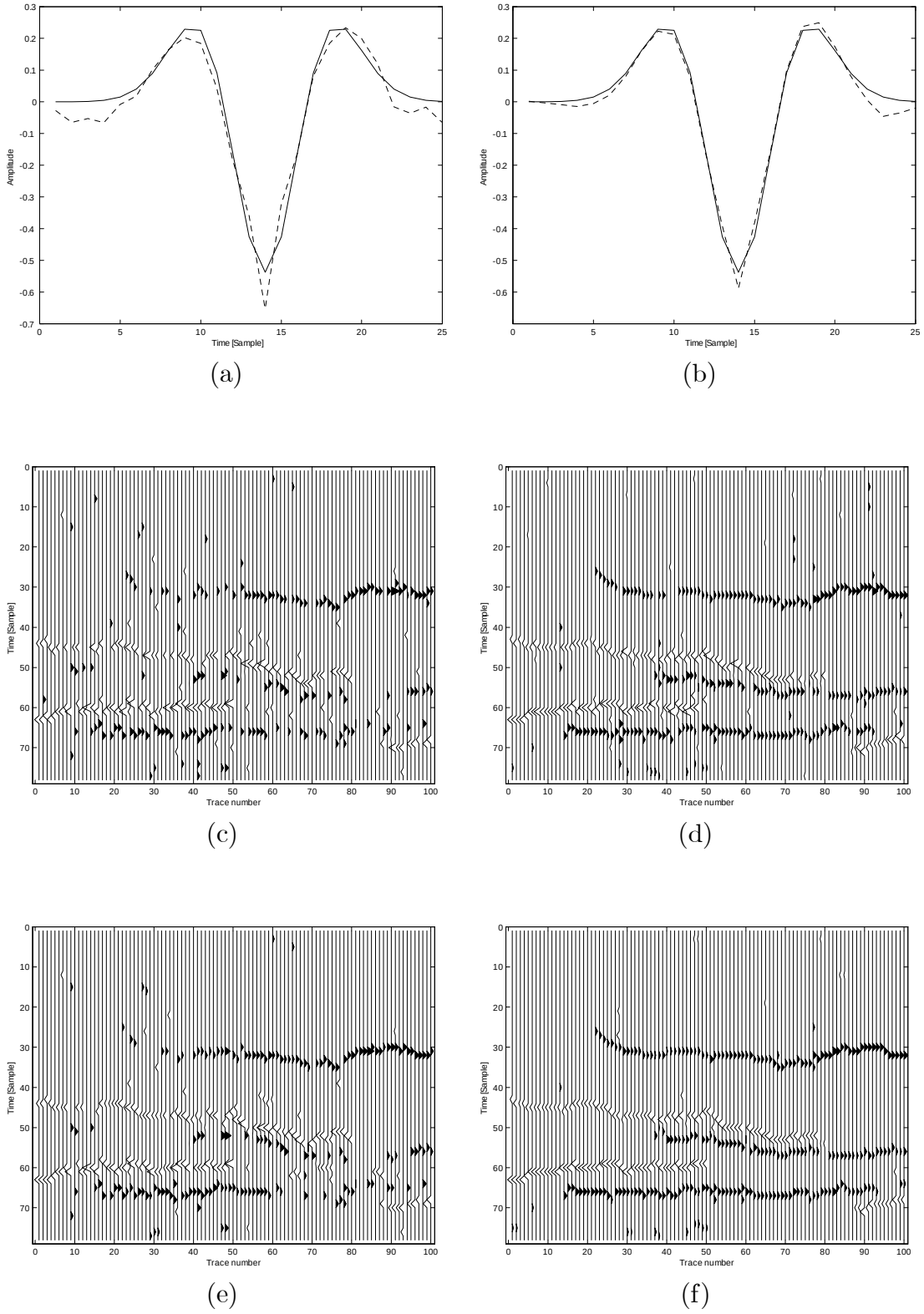

(a) (b) (c) (d) (e) (f)

Figure 3.3: Synthetic 2D data MC I results: (a) True wavelet (solid) and its estimate (dotted) for SNR=0 dB. (b) True wavelet (solid) and its estimate (dotted) for SNR=5 dB. (c) Single-channel decovnoltuion results for SNR=0 dB. (c) Single-channel decovnoltuion results for SNR=5 dB. (e) MC I results for SNR=0 dB. (e) MC I results for SNR=5 dB.

with half their amplitude. For theses reflectors a penalty of 0.5 was added to both the missed and false detection measures. The new loss functions are:

$$\begin{aligned} L_2^{miss+false} &= D + N_2^{miss} + N_2^{false} \\ L_2^{miss} &= \|\hat{\mathbf{x}} - \mathbf{x}\|_1 + N_2^{miss} \\ L_2^{false} &= \|\hat{\mathbf{x}} - \mathbf{x}\|_1 + N_2^{false} \end{aligned} \tag{3.13}$$

where $D = \sum_n \left|\hat{r}(n) + \frac{1}{2}\hat{r}(n-1) + \frac{1}{2}\hat{r}(n+1) - r(n)\right|$ is a difference measure, $N_2^{miss} = N^{miss} - \frac{1}{2} \times \#\{n : r(n) \neq 0,\, \hat{r}(n) = 0,\, \hat{r}(n-1) \neq 0 \text{ or } \hat{r}(n+1) \neq 0\}$ is a missed detection measure and $N_2^{false} = N^{false} - \frac{1}{2} \times \#\{n : \hat{r}(n) \neq 0,\, r(n) = 0,\, r(n-1) \neq 0 \text{ or } r(n+1) \neq 0\}$ is a false detection measure. Since we are dealing with 2D reflectivity signals, we calculated the loss function for their column stack forms. We also normalized L^{SSQ} by the L_2 norm of the column stack forms and normalized the rest of the loss functions by the number of reflectors contained in the column stack forms. The means and standard deviations of the loss functions calculated for the estimates obtained by single-channel deconvolution and the MC I algorithm are shown in percents in Table 3.2

It can be seen that for both SNR levels, and for all the loss functions, the mean values calculated for the estimates of the MC I algorithm are smaller then the respective mean values calculated for the estimates of the single-channel deconvolution algorithm. This implies that the MC I algorithm produces better results than the single-channel algorithm. It can also be seen that lower mean values of the loss functions are measured for all the estimates with the higher SNR, meaning

Table 3.2: Comparison between the quality of restoration of the single-channel deconvolution (SC) and the MC I algorithms

SNR (dB)	0		5	
	SC	MC I	SC	MC I
$L^{miss+false}$	207.13 (13.76)	185.57 (18.01)	112.36 (10.89)	81.15 (13.61)
L^{miss}	167.94 (9.51)	148.91 (13.54)	88.55 (7.95)	64.33 (10.02)
L^{false}	145.55 (11.82)	131.9 (14.08)	79.76 (8.38)	57.67 (10.11)
L^{SSQ}	101.35 (4.46)	94.1 (6.23)	67.8 (4.32)	54.01 (5.68)
$L_2^{miss+false}$	146.65 (8.99)	123.08 (11.64)	76.38 (6.39)	54.13 (8.24)
L_2^{miss}	118.4 (5.69)	98.16 (8.46)	59.78 (4.46)	42.95 (5.87)
L_2^{false}	96.05 (8.06)	81.17 (8.93)	51.14 (4.82)	36.54 (5.8)

that both algorithms performed better when the noise level was low.

3.8.2 Real Data

We applied the proposed parameter estimation method to the real seismic data used in Section 2.5.2, and redepicted here in Fig 3.5(a). The estimated wavelet is shown in Fig. 3.4 and the estimated parameters are presented in Table 3.3. As expected, the estimates obtained here for the parameters $\boldsymbol{\theta} = (\mathbf{h}, \lambda, \sigma_r, \sigma_w)$ are identical to the ones obtained in the previous chapter.

Table 3.3: Real data example: parameters estimated for the real data

λ	σ_r	σ_w	a	$\mu^{/}$	μ^{-}	$\mu^{\backslash}$	ε
0.0385	3.9451	0.7008	0.9007	0.0015	0.011	0.0009	0.0254

The estimated parameters were employed by the deconvolution scheme of the MC I algorithm. Similarly to the case of the synthetic data, we used the single-channel deconvolution results, obtained for this data set in Chapter 2, for comparison reasons. The reflectivity sections obtained by single-channel deconvolution and MC I are shown in Figs. 3.5(b) and (c) respectively. Comparing these re-

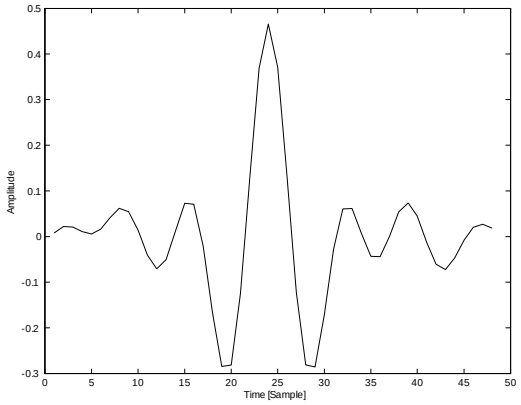

Figure 3.4: Real data estimated seismic wavelet.

flectivity sections, it can be seen that the estimates obtained by MC I contain layer boundaries which are more continuous and smooth than the ones obtained by the single-channel deconvolution. This algorithm also manages to detect parts of the layers that the single-channel deconvolution missed. Note that since the true reflectivity section is unknown, the loss functions (3.12) and (3.13) cannot be used to assess the performance of the proposed algorithms on real data.

3.9 Summary

We have proposed a recursive causal multichannel blind deconvolution algorithm. This algorithm is based on the MBG I reflectivity prior model and carry out the deconvolution iteratively. It employs in each iteration a modified MPM algorithm which estimates a reflectivity column from the corresponding observed trace and an estimate of the preceding reflectivity column. The proposed algorithm, which takes into account the spatial dependency between neighboring traces in the decon-

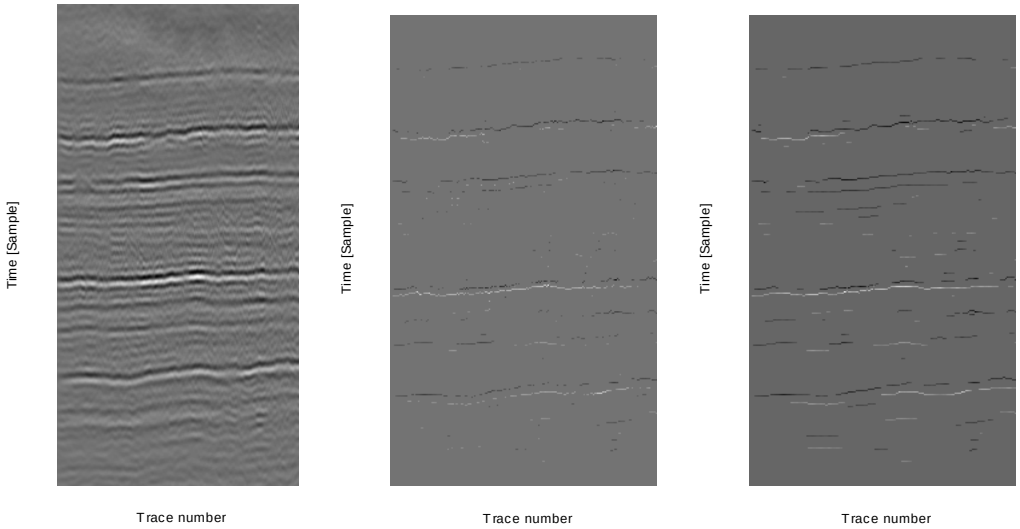

(a) (b) (c)

Figure 3.5: Real data MC I results: (a) Seismic trace. (b) Single-channel deconvolution results. (c) MC I results.

volution process, showed better performance than a single-channel deconvolution algorithm, for synthetic and real data.

Chapter 4

Recursive Noncausal Multichannel Blind Deconvolution

4.1 Introduction

The algorithm proposed in the previous chapter, iteratively deconvolves the seismic data, while taking into account the dependency between each reflectivity column and its preceding neighbor. On the other hand, it doesn't take into account the dependency between each reflectivity column and its subsequent neighbor, although the latter is also very informative about the former. The algorithm proposed in this chapter, is an extended version of the first proposed algorithm, and uses the same reflectivity model and parameter estimation method. However, it performs the deconvolution in a recursive noncausal manner, and employs in each iteration

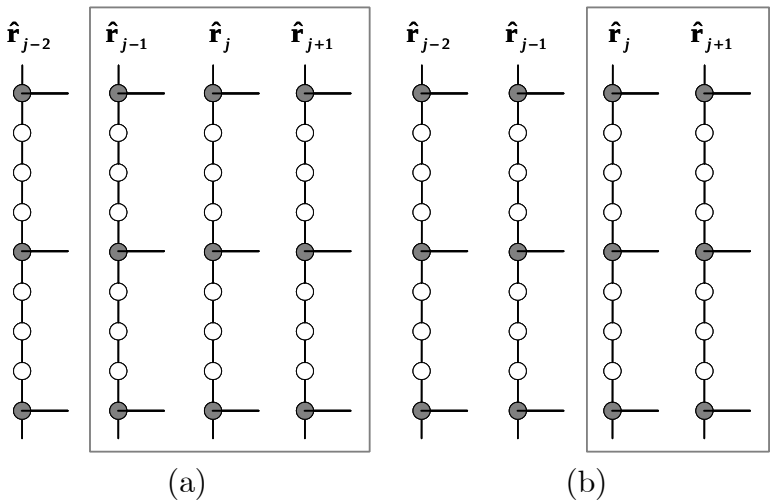

Figure 4.1: Two proposed estimation windows

a further modified MPM algorithm which takes into account the dependency between each reflectivity column and both the preceding and subsequent neighbors. The proposed algorithm is applied to both simulated and real data, and is shown to produces better results than the ones obtained by both the first algorithm and the single-channel algorithm of Rosec et al. This chapter is organized as follows: In Sections 4.2-4.4 we present the proposed deconvolution scheme, the further modified version of the MPM algorithm and the Gibbs samplers it utilizes. We present simulated and real data experimental results in Section 4.5, and finally we summarize this chapter in Section 4.6.

4.2 Deconvolution Scheme

Our goal is to improve the performance of the first proposed algorithm, by taking into account information from both preceding and subsequent traces in the deconvolution process of each trace. More specifically, we wish to utilize estimates of both $\mathbf{r}_{j-1}$ and $\mathbf{r}_{j+1}$, in the estimation process of $\mathbf{r}_j$. However, an estimate of $\mathbf{r}_{j+1}$ is not available from previous iterations in the jth iteration, in which $\mathbf{r}_j$ is estimated. Therefore, instead of estimating only $\mathbf{r}_j$ in the jth iteration, we simultaneously estimate all the reflectivity columns inside a window which contains both $\mathbf{r}_j$ and $\mathbf{r}_{j+1}$. This way, the dependency between $\mathbf{r}_j$ and $\mathbf{r}_{j+1}$ is taken into account when the former is estimated. In each iteration besides the last, only the estimate of $\mathbf{r}_j$ is kept out of the obtained estimates. The estimate of the $\mathbf{r}_{j+1}$ is discarded, as this column will be reestimated in the next iteration. It is kept only in the last iteration, as the estimate of the last column in the 2D reflectivity section $\mathbf{r}_J$.

We propose two kinds of estimation windows: the first window, shown in Fig. 4.1(a), includes $\mathbf{r}_j$ and the reflectivity columns preceding and subsequent it, while the second window, shown in Fig. 4.1(b), includes only $\mathbf{r}_j$ and the subsequent reflectivity column. When the first window is used, $\mathbf{r}_{j-1}$ is reestimated along with the rest of the columns in the window, although it was already estimated in the previous iteration. This way we insure that $\hat{\mathbf{r}}_j$ will be influenced only by observations in its close environment and prevent errors in estimates of previous reflectivity columns from defusing onward. On the other hand, when the second window is used, only $\mathbf{r}_j$ and $\mathbf{r}_{j+1}$ are estimated, conditionally to the estimate of $\mathbf{r}_{j-1}$ obtained in the previous iteration. In this case, the computational burden

is reduced, since only two reflectivity columns are estimated in each iteration. Also, information from preceding traces is taken into account through $\hat{\mathbf{r}}_{j-1}$ in the estimation process of $\mathbf{r}_j$, which results in a more continuous estimate of the 2D reflectivity section. In the sequel, we use only the second type of window, as simulation results (not reported her) showed better deconvolution results are obtained with it, than with the first window. Extending the deconvolution process derived next to the case where the first window type or a larger window size are used, is straightforward, at the cost of a larger computational burden.

We next define the following vectors:

$\bar{\mathbf{y}}_j = \left[\mathbf{y}_j^T, \mathbf{y}_{j+1}^T\right]^T$, $\bar{\mathbf{r}}_j = \left[\mathbf{r}_j^T, \mathbf{r}_{j+1}^T\right]^T$, $\bar{\mathbf{q}}_j = \left[\mathbf{q}_j^T, \mathbf{q}_{j+1}^T\right]^T$, $\bar{\mathbf{t}}_{j-1}^{/} = \left[\left(\mathbf{t}_{j-1}^{/}\right)^T, \left(\mathbf{t}_j^{/}\right)^T\right]^T$, $\bar{\mathbf{t}}_{j-1}^{-} = \left[\left(\mathbf{t}_{j-1}^{-}\right)^T, \left(\mathbf{t}_j^{-}\right)^T\right]^T$, $\bar{\mathbf{t}}_{j-1}^{\backslash} = \left[\left(\mathbf{t}_{j-1}^{\backslash}\right)^T, \left(\mathbf{t}_j^{\backslash}\right)^T\right]^T$, $j = 1, ..., J-1$,

where $\mathbf{t}_0^{/} = \mathbf{t}_0^{/} = \mathbf{t}_0^{/} = \mathbf{0}_{N_r \times 1}$ and $\mathbf{0}_{N_r \times 1}$ denotes a vector of N_r zeros. Using these concatenated vectors in the deconvolution process allows us to simultaneously estimate the amplitude, location and transition variables associated with both $\mathbf{r}_j$ and $\mathbf{r}_{j+1}$. The deconvolution is carried out iteratively, using the following maximization procedure:

$$(1)\ \text{First column: } \left(\widehat{\bar{\mathbf{r}}}_1, \widehat{\bar{\mathbf{q}}}_1\ , \widehat{\bar{\mathbf{t}}}_0^{/}\ , \widehat{\bar{\mathbf{t}}}_0^{-}\ , \widehat{\bar{\mathbf{t}}}_0^{\backslash}\right) = \underset{\bar{\mathbf{r}}_1, \bar{\mathbf{q}}_1, \bar{\mathbf{t}}_0^{/}, \bar{\mathbf{t}}_0^{-}, \bar{\mathbf{t}}_0^{\backslash}}{\text{argmax}}\ p\left(\bar{\mathbf{r}}_1, \bar{\mathbf{q}}_1,\ \bar{\mathbf{t}}_0^{/},\ \bar{\mathbf{t}}_0^{-},\ \bar{\mathbf{t}}_0^{\backslash}\,|\bar{\mathbf{y}}_1\right) \tag{4.1}$$

$$(2)\ j \in [2, J-1] : \left(\widehat{\bar{\mathbf{r}}}_j, \widehat{\bar{\mathbf{q}}}_j,\ \widehat{\bar{\mathbf{t}}}_{j-1}^{/},\ \widehat{\bar{\mathbf{t}}}_{j-1}^{-},\ \widehat{\bar{\mathbf{t}}}_{j-1}^{\backslash}\right)$$
$$= \underset{\bar{\mathbf{r}}_j, \bar{\mathbf{q}}_j, \bar{\mathbf{t}}_{j-1}^{/}, \bar{\mathbf{t}}_{j-1}^{-}, \bar{\mathbf{t}}_{j-1}^{\backslash}}{\text{argmax}}\ p\left(\bar{\mathbf{r}}_j, \bar{\mathbf{q}}_j,\ \bar{\mathbf{t}}_{j-1}^{/},\ \bar{\mathbf{t}}_{j-1}^{-},\ \bar{\mathbf{t}}_{j-1}^{\backslash}\,|\bar{\mathbf{y}}_j,\ \hat{\mathbf{r}}_{j-1},\ \hat{\mathbf{q}}_{j-1}\right) \tag{4.2}$$

Similarly to the deconvolution scheme of the first proposed algorithm, a single partial criterion is optimized in each iteration. Direct optimization of these partial criteria is practically impossible, since it requires examination of all the possible configurations of $\bar{\mathbf{q}}_j, \bar{\mathbf{t}}_{j-1}^{/}, \bar{\mathbf{t}}_{j-1}^{-}, \bar{\mathbf{t}}_{j-1}^{\backslash}$, whose number ranges from 2^{2N_r} to 8^{2N_r}. Instead, we apply a further modified version of the MPM algorithm to these partial criteria. This MPM algorithm estimates in the first iteration $\bar{\mathbf{t}}_0^{/}, \bar{\mathbf{t}}_0^{-}, \bar{\mathbf{t}}_0^{\backslash}, \bar{\mathbf{q}}_1$ and $\bar{\mathbf{r}}_1$ from $\bar{\mathbf{y}}_1$, and estimates in the jth iteration, $j \in [2, J-1]$, $\bar{\mathbf{t}}_{j-1}^{/}, \bar{\mathbf{t}}_{j-1}^{-}, \bar{\mathbf{t}}_{j-1}^{\backslash}, \bar{\mathbf{q}}_j$ and $\bar{\mathbf{r}}_j$ from $\bar{\mathbf{y}}_j$, $\hat{\mathbf{r}}_{j-1}$ and $\hat{\mathbf{q}}_{j-1}$. The first N_r samples of the estimates of $\bar{\mathbf{r}}_j, \bar{\mathbf{q}}_j, \bar{\mathbf{t}}_{j-1}^{/}, \bar{\mathbf{t}}_{j-1}^{-}, \bar{\mathbf{t}}_{j-1}^{\backslash}$, $j \in [1, J-1]$ are kept as the desired estimates $\hat{\mathbf{r}}_j, \hat{\mathbf{q}}_j, \hat{\mathbf{t}}_{j-1}^{/}, \hat{\mathbf{t}}_{j-1}^{-}, \hat{\mathbf{t}}_{j-1}^{\backslash}$. In $J-1$th iteration the last N_r samples of the estimates are also kept as $\hat{\mathbf{r}}_J, \hat{\mathbf{q}}_J, \hat{\mathbf{t}}_{J-1}^{/}, \hat{\mathbf{t}}_{J-1}^{-}, \hat{\mathbf{t}}_{J-1}^{\backslash}$.

The MPM algorithm employs two different Gibbs samplers in the estimation process of $\mathbf{r}_1$ and $\mathbf{r}_j$, $j \in [1, J-1]$. We describe these Gibbs samplers next.

4.3 Gibbs samplers

4.3.1 First reflectivity column

In the estimation process of the first reflectivity column, we employ a Gibbs sampler to generate samples of $\bar{\mathbf{r}}_1, \bar{\mathbf{q}}_1, \bar{\mathbf{t}}_0^{/}, \bar{\mathbf{t}}_0^{-}, \bar{\mathbf{t}}_0^{\backslash}$ from the joint distribution $p\left(\bar{\mathbf{r}}_1, \bar{\mathbf{q}}_1, \bar{\mathbf{t}}_0^{/}, \bar{\mathbf{t}}_0^{-}, \bar{\mathbf{t}}_0^{\backslash} | \bar{\mathbf{y}}_1\right)$. Instead of sampling directly from this joint distribution, the Gibbs sampler iteratively samples from the conditional distributions of $\bar{r}_{k,1}$, $\bar{q}_{k,1}$, $\bar{t}_{k,0}^{/}$, $\bar{t}_{k,0}^{-}$ and $\bar{t}_{k,0}^{\backslash}$. The first N_r samples of $\bar{\mathbf{t}}_0^{/}, \bar{\mathbf{t}}_0^{-}, \bar{\mathbf{t}}_0^{\backslash}$ equal zero and the first N_r samples of $\bar{\mathbf{r}}_1, \bar{\mathbf{q}}_1$ are sampled from:

1. $p\left(r_{k,1}, q_{k,1} \left| \mathbf{y}_1, \mathbf{r}_{-k,1}, \mathbf{q}_{-k,1}, \mathbf{r}_2, \mathbf{q}_2, \mathbf{t}_1^{/}, \mathbf{t}_1^{-}, \mathbf{t}_1^{\backslash}\right.\right) \quad \sim \quad \lambda_{k,1}^{f} N\left(m_{k,1}^{f}, V_{k,1}^{f}\right) \quad + \left(1 - \lambda_{k,1}^{f}\right) \delta\left(r_{k,j}\right)$

where the derivation of $\lambda_{k,j}^{f}$, $m_{k,j}^{f}$ and $V_{k,j}^{f}$ can be found in Section A.3 of the appendix. The last N_r samples of $\bar{\mathbf{r}}_1, \bar{\mathbf{q}}_1, \bar{\mathbf{t}}_0^{/}, \bar{\mathbf{t}}_0^{-}, \bar{\mathbf{t}}_0^{\backslash}$ are sampled from:

1. $p\left(t_{k-N_r,1}^{/} \left| \mathbf{r}_2, \mathbf{q}_2, \mathbf{t}_{-(k-N_r),1}^{/}, \mathbf{t}_1^{-}, \mathbf{t}_1^{\backslash}, \mathbf{r}_1, \mathbf{q}_1\right.\right) \sim B\left(\mu_{k-N_r,1}^{/}\right)$
2. $p\left(t_{k-N_r,1}^{-} \left| \mathbf{r}_2, \mathbf{q}_2, \mathbf{t}_1^{/}, \mathbf{t}_{-(k-N_r),1}^{-}, \mathbf{t}_1^{\backslash}, \mathbf{r}_1, \mathbf{q}_1\right.\right) \sim B\left(\mu_{k-N_r,1}^{-}\right)$
3. $p\left(t_{k-N_r,1}^{\backslash} \left| \mathbf{r}_2, \mathbf{q}_2, \mathbf{t}_1^{/}, \mathbf{t}_1^{-}, \mathbf{t}_{-(k-N_r),1}^{\backslash}, \mathbf{r}_1, \mathbf{q}_1\right.\right) \sim B\left(\mu_{k-N_r,1}^{\backslash}\right)$
4. $p\left(r_{k-N_r,2}, q_{k-N_r,2} \left| \mathbf{y}_2, \mathbf{r}_{-(k-N_r),2}, \mathbf{q}_{-(k-N_r),2}, \mathbf{t}_1^{/}, \mathbf{t}_1^{-}, \mathbf{t}_1^{\backslash}, \mathbf{r}_1\right.\right)$
   $\sim \lambda_{k-N_r,2}^{b} N\left(m_{k-N_r,2}^{b}, V_{k-N_r,2}^{b}\right) + \left(1 - \lambda_{k-N_r,2}^{b}\right) \delta\left(r_{k-N_r,2}\right)$

For the simulation of the vectors $\bar{\mathbf{r}}_1$, $\bar{\mathbf{q}}_1$, $\bar{\mathbf{t}}_0^{/}, \bar{\mathbf{t}}_0^{-}$ and $\bar{\mathbf{t}}_0^{\backslash}$, the Gibbs sampler follows these steps iteratively:

1. Initialization: choice of $\bar{\mathbf{r}}_1^{(0)}, \bar{\mathbf{q}}_1^{(0)}, \bar{\mathbf{t}}_0^{/\,(0)}, \bar{\mathbf{t}}_0^{-\,(0)}, \bar{\mathbf{t}}_0^{\setminus\,(0)}$.

2. For $i = 1, ..., I$

   For $k = 1, ..., N_r$

   - detection step:
     - compute $\lambda_{k,1}^f$ using (A.40) and simulate $\bar{q}_{k,1}^{(i)} \sim B\left(\lambda_{k,1}^f\right)$
   - estimation step:
     - simulate $\bar{r}_{k,1}^{(i)}$ where $\bar{r}_{k,1}^{(i)} \sim N\left(m_{k,1}^f, V_{k,1}^f\right)$ if $\bar{q}_{k,j} = 1$ and $\bar{r}_{k,1}^{(i)} = 0$ if $\bar{q}_{k,1}^{(i)} = 0$.

   For $k = N_r + 1, .., 2N_r$

   - detection step:
     - compute $\mu_{k-N_r,1}^{/}$ using (A.18) and simulate $\bar{t}_{k,0}^{/\,(i)} \sim B\left(\mu_{k-N_r,1}^{/}\right)$
     - compute $\mu_{k-N_r,1}^{-}$ using (A.24) and simulate $\bar{t}_{k,0}^{-\,(i)} \sim B\left(\mu_{k-N_r,1}^{-}\right)$
     - compute $\mu_{k-N_r,1}^{\setminus}$ using (A.30) and simulate $\bar{t}_{k,0}^{\setminus\,(i)} \sim B\left(\mu_{k-N_r,1}^{\setminus}\right)$
     - compute $\lambda_{k-N_r,2}^b$ using (A.8) and simulate $\bar{q}_{k,1}^{(i)} \sim B\left(\lambda_{k-N_r,2}^b\right)$
   - estimation step:
     - simulate $\bar{r}_{k,1}^{(i)}$ where $\bar{r}_{k,1}^{(i)} \sim N\left(m_{k-N_r,2}^b, V_{k-N_r,2}^b\right)$ if $\bar{q}_{k,1}^{(i)} = 1$ and $\bar{r}_{k,1}^{(i)} = 0$ if $\bar{q}_{k,1}^{(i)} = 0$.

4.3.2 jth reflectivity column, $j \in [1, J-1]$

In the estimation process of the jth reflectivity column, $j \in [2, J-1]$, we employ a Gibbs sampler to generate samples of $\bar{\mathbf{r}}_j, \bar{\mathbf{q}}_j, \bar{\mathbf{t}}^{/}_{j-1}, \bar{\mathbf{t}}^{-}_{j-1}, \bar{\mathbf{t}}^{\backslash}_{j-1}$ from the joint distribution $p\left(\bar{\mathbf{r}}_j, \bar{\mathbf{q}}_j, \bar{\mathbf{t}}^{/}_{j-1}, \bar{\mathbf{t}}^{-}_{j-1}, \bar{\mathbf{t}}^{\backslash}_{j-1} | \bar{\mathbf{y}}_j, \hat{\mathbf{r}}_{j-1}, \hat{\mathbf{q}}_{j-1}\right)$. Instead of sampling directly from this joint distribution, the Gibbs sampler iteratively samples from the conditional distributions of $\bar{r}_{k,j}, \bar{q}_{k,j}, \bar{t}^{/}_{k,j-1}\bar{t}^{-}_{k,j-1}$ and $\bar{t}^{\backslash}_{k,j-1}$. The first N_r samples of $\bar{\mathbf{r}}_j, \bar{\mathbf{q}}_j, \bar{\mathbf{t}}^{/}_{j-1}, \bar{\mathbf{t}}^{-}_{j-1}, \bar{\mathbf{t}}^{\backslash}_{j-1}$ are sampled from:

1. $p\left(t^{/}_{k,j-1} \middle| \mathbf{r}_j, \mathbf{q}_j, \mathbf{t}^{/}_{-k,j-1}, \mathbf{t}^{-}_{j-1}, \mathbf{t}^{\backslash}_{j-1}, \hat{\mathbf{r}}_{j-1}, \hat{\mathbf{q}}_{j-1}\right) \sim B\left(\mu^{/}_{k,j-1}\right)$
2. $p\left(t^{-}_{k,j-1} \middle| \mathbf{r}_j, \mathbf{q}_j, \mathbf{t}^{/}_{j-1}, \mathbf{t}^{-}_{-k,j-1}, \mathbf{t}^{\backslash}_{j-1}, \hat{\mathbf{r}}_{j-1}, \hat{\mathbf{q}}_{j-1}\right) \sim B\left(\mu^{-}_{k,j-1}\right)$
3. $p\left(t^{\backslash}_{k,j-1} \middle| \mathbf{r}_j, \mathbf{q}_j, \mathbf{t}^{/}_{j-1}, \mathbf{t}^{-}_{j-1}, \mathbf{t}^{\backslash}_{-k,j-1}, \hat{\mathbf{r}}_{j-1}, \hat{\mathbf{q}}_{j-1}\right) \sim B\left(\mu^{\backslash}_{k,j-1}\right)$
4. $p\left(r_{k,j}, q_{k,j} \middle| \mathbf{y}_j, \mathbf{r}_{-k,j}, \mathbf{q}_{-k,j}, \mathbf{t}^{/}_{j-1}, \mathbf{t}^{-}_{j-1}, \mathbf{t}^{\backslash}_{j-1}, \hat{\mathbf{r}}_{j-1}, \mathbf{r}_{j+1}, \mathbf{q}_{j+1}, \mathbf{t}^{/}_{j}, \mathbf{t}^{-}_{j}, \mathbf{t}^{\backslash}_{j}\right)$
   $\sim \lambda^m_{k,j} N\left(m^m_{k,j}, V^m_{k,j}\right) + \left(1 - \lambda^m_{k,j}\right) \delta\left(r_{k,j}\right)$

where the derivation of $\lambda^m_{k,j}$, $m^m_{k,j}$ and $V^m_{k,j}$ can be found in Section A.4 of the appendix. The last N_r samples of $\bar{\mathbf{r}}_j, \bar{\mathbf{q}}_j, \bar{\mathbf{t}}^{/}_{j-1}, \bar{\mathbf{t}}^{-}_{j-1}, \bar{\mathbf{t}}^{\backslash}_{j-1}$ are sampled from:

1. $p\left(t^{/}_{k-N_r,j} \middle| \mathbf{r}_{j+1}, \mathbf{q}_{j+1}, \mathbf{t}^{/}_{-(k-N_r),j}, \mathbf{t}^{-}_{j}, \mathbf{t}^{\backslash}_{j}, \mathbf{r}_j, \mathbf{q}_j\right) \sim B\left(\mu^{/}_{k-N_r,j}\right)$
2. $p\left(t^{-}_{k-N_r,j} \middle| \mathbf{r}_{j+1}, \mathbf{q}_{j+1}, \mathbf{t}^{/}_{j}, \mathbf{t}^{-}_{-(k-N_r),j}, \mathbf{t}^{\backslash}_{j}, \mathbf{r}_j, \mathbf{q}_j\right) \sim B\left(\mu^{-}_{k-N_r,j}\right)$
3. $p\left(t^{\backslash}_{k-N_r,j} \middle| \mathbf{r}_{j+1}, \mathbf{q}_{j+1}, \mathbf{t}^{/}_{,j}, \mathbf{t}^{-}_{j}, \mathbf{t}^{\backslash}_{-(k-N_r),j}, \mathbf{r}_j, \mathbf{q}_j\right) \sim B\left(\mu^{\backslash}_{k-N_r,j}\right)$
4. $p\left(r_{k-N_r,j+1}, q_{k-N_r,j+1} \middle| \mathbf{y}_{j+1}, \mathbf{r}_{-(k-N_r),j+1}, \mathbf{q}_{-(k-N_r),j+1}, \mathbf{t}^{/}_{j}, \mathbf{t}^{-}_{j}, \mathbf{t}^{\backslash}_{j}, \mathbf{r}_j\right)$
   $\sim \lambda^b_{k-N_r,j+1} N\left(m^b_{k-N_r,j+1}, V^b_{k-N_r,j+1}\right) + \left(1 - \lambda^b_{k-N_r,j+1}\right) \delta\left(r_{k-N_r,j+1}\right)$

For the simulation of the vectors $\bar{\mathbf{r}}_j, \bar{\mathbf{q}}_j, \bar{\mathbf{t}}^{/}_{j-1}, \bar{\mathbf{t}}^{-}_{j-1}$ and $\bar{\mathbf{t}}^{\backslash}_{j-1}$, the Gibbs sampler follows these steps iteratively:

1. Initialization: choice of $\bar{\mathbf{r}}_j^{(0)}$, $\bar{\mathbf{q}}_j^{(0)}, \bar{\mathbf{t}}^{/\,(0)}_{j-1}, \bar{\mathbf{t}}^{-\,(0)}_{j-1}, \bar{\mathbf{t}}^{\backslash\,(0)}_{j-1}$.

2. For $i = 1, ..., I$

   For $k = 1, ..., N_r$

   - detection step:
     - compute $\mu^{/}_{k,j-1}$ using (A.18) and simulate $\bar{t}^{/\,(i)}_{k,j-1} \sim B\left(\mu^{/}_{k,j-1}\right)$
     - compute $\mu^{-}_{k,j-1}$ using (A.24) and simulate $\bar{t}^{-\,(i)}_{k,j-1} \sim B\left(\mu^{-}_{k,j-1}\right)$
     - compute $\mu^{\backslash}_{k,j-1}$ using (A.30) and simulate $\bar{t}^{\backslash\,(i)}_{k,j-1} \sim B\left(\mu^{\backslash}_{k,j-1}\right)$
     - compute $\lambda^{m}_{k,j}$ using (A.48) and simulate $\bar{q}^{(i)}_{k,j} \sim B\left(\lambda^{m}_{k,j}\right)$
   - estimation step:
     - simulate $\bar{r}^{(i)}_{k,j}$ where $\bar{r}^{(i)}_{k,j} \sim N\left(m^{m}_{k,j}, V^{m}_{k,j}\right)$ if $\bar{q}_{k,j} = 1$ and $\bar{r}^{(i)}_{k,j} = 0$ if $\bar{q}^{(i)}_{k,j} = 0$.

   For $k = N_r + 1, .., 2N_r$

   - detection step:
     - compute $\mu^{/}_{k-N_r,j}$ using (A.18) and simulate $\bar{t}^{/\,(i)}_{k,j-1} \sim B\left(\mu^{/}_{k-N_r,j}\right)$
     - compute $\mu^{-}_{k-N_r,j}$ using (A.24) and simulate $\bar{t}^{-\,(i)}_{k,j-1} \sim B\left(\mu^{-}_{k-N_r,j}\right)$
     - compute $\mu^{\backslash}_{k-N_r,j}$ using (A.30) and simulate $\bar{t}^{\backslash\,(i)}_{k,j-1} \sim B\left(\mu^{\backslash}_{k-N_r,j}\right)$
     - compute $\lambda^{b}_{k-N_r,j+1}$ using (A.8) and simulate $\bar{q}^{(i)}_{k,j} \sim B\left(\lambda^{b}_{k-N_r,j+1}\right)$

- estimation step:
  - simulate $\bar{r}_{k,j}^{(i)}$ where $\bar{r}_{k,j}^{(i)} \sim N\left(m_{k-N_r,j+1}^{b}, V_{k-N_r,j+1}^{b}\right)$ if $\bar{q}_{k,j} = 1$ and $\bar{r}_{k,j}^{(i)} = 0$ if $\bar{q}_{k,j}^{(i)} = 0$.

4.4 MPM algorithm

The second proposed algorithm employs a further modified MPM algorithm. This MPM algorithm estimates $\bar{\mathbf{r}}_1, \bar{\mathbf{q}}_1, \bar{\mathbf{t}}_0^{/}, \bar{\mathbf{t}}_0^{-}\bar{\mathbf{t}}_0^{\backslash}$ in the first iteration, and estimates $\bar{\mathbf{r}}_j, \bar{\mathbf{q}}_j, \bar{\mathbf{t}}_{j-1}^{/}, \bar{\mathbf{t}}_{j-1}^{-}\bar{\mathbf{t}}_{j-1}^{\backslash}$, $j \in [2, J-1]$ in the following iterations. It uses the two versions of the Gibbs sampler described in the previous section to generate realizations of $\bar{\mathbf{r}}_j, \bar{\mathbf{q}}_j, \bar{\mathbf{t}}_{j-1}^{/}, \bar{\mathbf{t}}_{j-1}^{-}$ and $\bar{\mathbf{t}}_{j-1}^{\backslash}$, where the first I_0 iterations are considered a learning period. Only the samples $\left(\bar{\mathbf{r}}_j^{(i)}, \bar{\mathbf{q}}_j^{(i)}, \bar{\mathbf{t}}_{j-1}^{/\,(i)}, \bar{\mathbf{t}}_{j-1}^{-\,(i)}, \bar{\mathbf{t}}_{j-1}^{\backslash\,(i)}\right)$ produced in the subsequent steady state period $I_0 < i \leq I$ are used to first estimate each of $\bar{q}_{k,j}$, $\bar{t}_{k,j-1}^{/}$, $\bar{t}_{k,j-1}^{-}$, $\bar{t}_{k,j-1}^{\backslash}$ and then determine $\bar{r}_{k,j}$ conditionally to the estimate of $\bar{q}_{k,j}$.

The further modified MPM algorithm follows these steps iteratively:

1. For $i = 1, ..., I$ simulate $\left(\bar{\mathbf{t}}_{j-1}^{/\,(i)},\ \bar{\mathbf{t}}_{j-1}^{-\,(i)},\ \bar{\mathbf{t}}_{j-1}^{\backslash\,(i)},\ \bar{\mathbf{q}}_j^{(i)},\ \bar{\mathbf{r}}_j^{(i)}\right)$ using the Gibbs samplers.

2. For $k = 1, ..., 2N_r$

   - detection step:

$$\widehat{\bar{t}}_{k,j-1}^{/} = \begin{cases} 1, & \text{if } \frac{1}{I-I_0} \sum_{i=I_0+1}^{I} \bar{t}_{k,j-1}^{/\,(i)} > 0.5 \\ 0, & \text{otherwise} \end{cases},$$

$$\widehat{\bar{t}}_{k,j-1}^{-} = \begin{cases} 1, & \text{if } \frac{1}{I-I_0} \sum_{i=I_0+1}^{I} \bar{t}_{k,j-1}^{-(i)} > 0.5 \\ 0, & \text{otherwise} \end{cases},$$

$$\widehat{\bar{t}}_{k,j-1}^{\setminus} = \begin{cases} 1, & \text{if } \frac{1}{I-I_0} \sum_{i=I_0+1}^{I} \bar{t}_{k,j-1}^{\setminus(i)} > 0.5 \\ 0, & \text{otherwise} \end{cases},$$

$$\widehat{\bar{q}}_{k,j} = \begin{cases} 1, & \text{if } \frac{1}{I-I_0} \sum_{i=I_0+1}^{I} \bar{q}_{k,j}^{(i)} > 0.5 \\ 0, & \text{otherwise} \end{cases}$$

- estimation step:

$$\widehat{\bar{r}}_{k,j} = \begin{cases} \frac{\sum_{i=I_0+1}^{I} \tilde{q}_{k,j}^{(i)} \tilde{r}_{k,j}^{(i)}}{\sum_{i=I_0+1}^{I} \tilde{q}_{k,j}^{(i)}(k)}, & \text{if } \widehat{\bar{q}}_{k,j} = 1 \\ 0, & \text{otherwise} \end{cases}$$

4.5 Experimental Results

4.5.1 Synthetic data

We applied the second proposed algorithm, denoted hereafter as Multi-channel II (MC II), to each of the data sets synthesized in Section 2.5.1. Since the MC I and MC II algorithms employ the same parameter estimation method, we used as an input to the deconvolution scheme of MC II the parameters obtained in Section 3.8.1, which are presented in Table 3.1. Each column of the reflectivity sections estimated by MC II had gone through the same postprocessing procedure used by the algorithms presented in Chapters 2 and 3. The results of the MC II algorithm, obtained for the data sets with SNRs of 0 dB and 5 dB depicted in Figs. 2.2(a) and (b), are shown in Figs. 4.3(e) and (f), respectively. For comparison reasons

we depict here again the true reflectivity section (Fig. 4.2) and the reflectivity sections obtained for these data sets by single-channel deconvolution (Fig. 4.3 (a) and (b)) and the MC I algorithm (Fig. 4.3 (c) and (d)). Inspection of the results obtained by the MC II algorithm and the single-channel deconvolution algorithm reveals that for both SNRs the results obtained by the former are more continuous and contain less false detections and are generally closer to the true reflectivity than the results obtained by the latter.

We used the loss functions (3.12) and (3.13) in order to quantify the performances of the MC II algorithm and compare it to the performances of MC I and the single-channel algorithm. The means and standard deviations of the loss functions calculated for the estimates obtained by single-channel deconvolution and the MC I and MC II algorithms are shown in percents in Table 4.1. It can be seen that for both SNR levels, and for all the loss functions, the mean values calculated for the estimates of the MC II algorithm are smaller then the respective mean values calculated for the estimates of the single-channel deconvolution algorithm. This implies that the MC II algorithm produce better results than the single-channel algorithm. It can also be seen that for both SNR levels the MC II algorithm outperforms the MC I algorithm, and that the improvement is getting smaller as the SNR increases. Further, lower mean values of the loss functions are measured for all the estimates with the higher SNR, meaning that all the algorithms performed better when the noise level was low.

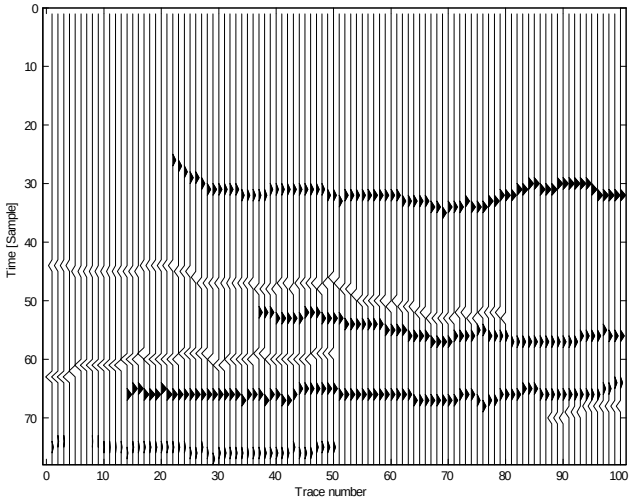

Figure 4.2: Synthetic 2D reflectivity section

Table 4.1: Comparison between the quality of restoration of the single channel deconvolution (SC), MC I and MC II algorithms.

SNR (dB)	0			5		
	SC	MC I	MC II	SC	MC I	MC II
$L^{miss+false}$	207.13 (13.76)	185.57 (18.01)	165.26 (16.67)	112.36 (10.89)	81.15 (13.61)	69.31 (10.42)
L^{miss}	167.94 (9.51)	148.91 (13.54)	132.2 (12.05)	88.55 (7.95)	64.33 (10.02)	54.81 (7.67)
L^{false}	145.55 (11.82)	131.9 (14.08)	117.96 (13.57)	79.76 (8.38)	57.67 (10.11)	49.35 (7.92)
L^{SSQ}	101.35 (4.46)	94.1 (6.23)	86.59 (6.06)	67.8 (4.32)	54.01 (5.68)	47.16 (5.31)
$L_2^{miss+false}$	146.65 (8.99)	123.08 (11.64)	106.65 (9.72)	76.38 (6.39)	54.13 (8.24)	46.48 (6.17)
L_2^{miss}	118.4 (5.69)	98.16 (8.46)	84.93 (6.49)	59.78 (4.46)	42.95 (5.87)	36.98 (4.34)
L_2^{false}	96.05 (8.06)	81.17 (8.93)	70.7 (7.99)	51.14 (4.82)	36.54 (5.8)	31.73 (4.54)

4.5.2 Real data

We applied the MC II algorithm to the real seismic data shown in Fig. 3.5(a), using the parameters estimated from this data in the Section 3.8.2. We compared the results, shown in Fig. 4.4(c) to the ones obtained for this data in the previous chapters by the single-channel and MC I algorithms, redepicted in Figs. 4.4(a) and (b), respectively. Similarly to the results obtained for the synthetic traces, the estimate produced by the MC II algorithm contain layer boundaries which are

more continuous and smooth than the results obtained by trace by trace single-channel deconvolution. It can also be seen that the estimates produced by the MC I and MC II algorithms are quite close, however the latter managed to recover parts of the layer boundaries missed by both the single-channel and first proposed algorithms.

4.6 Summary

We have proposed a recursive noncausal multichannel blind deconvolution algorithm , which is an extension of the first proposed algorithm, and uses the same reflectivity model and parameter estimation method. This algorithm employs in each iteration a further modified MPM algorithm which takes into account estimates of both the preceding and subsequent columns in the estimation process of the current reflectivity column. The second algorithm was applied to synthetic and real data traces, and was shown to produce better results than the ones obtained by the single-channel algorithm presented in Chapter 2 and the first proposed algorithm.

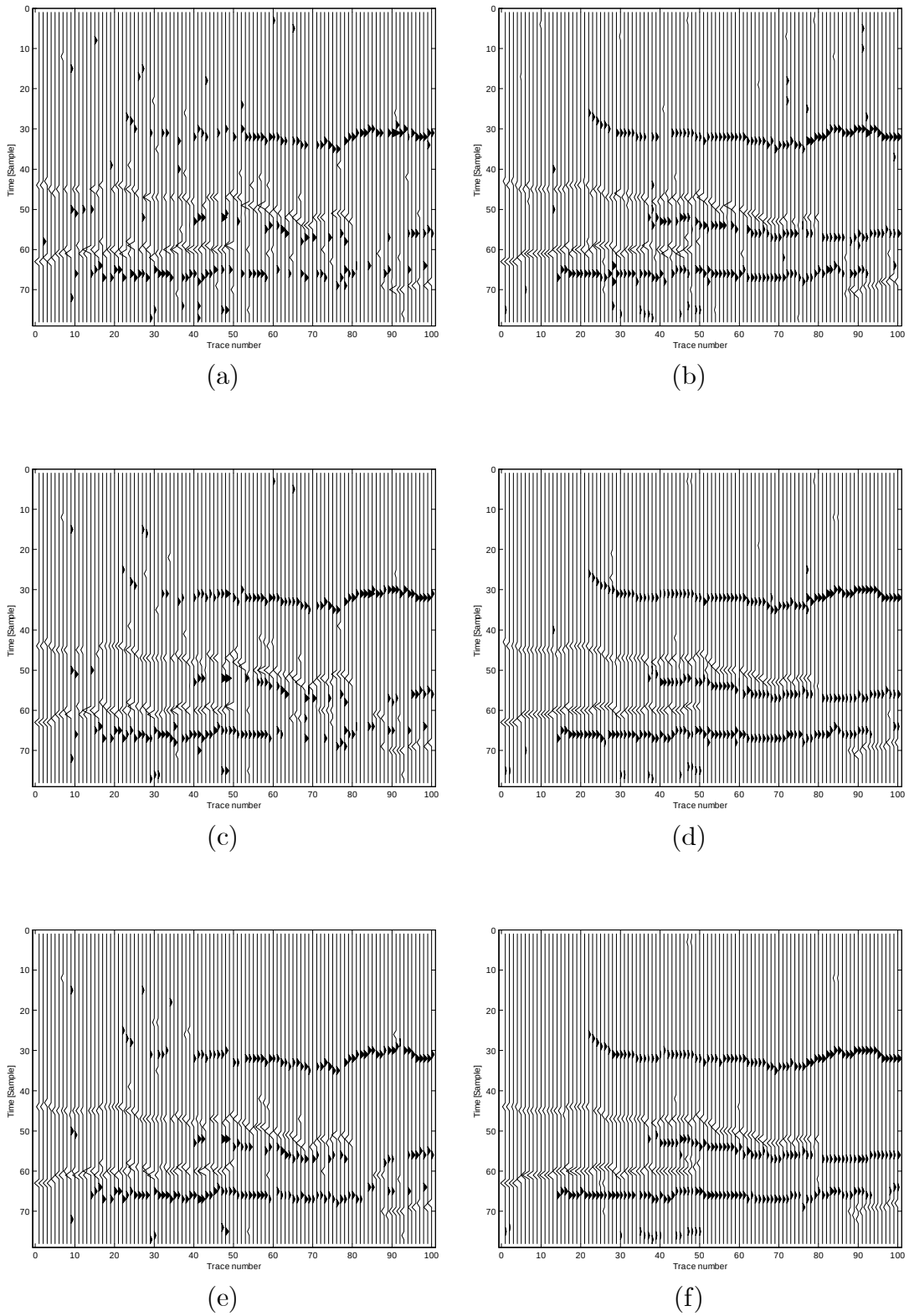

Figure 4.3: Synthetic 2D data MC II results: (a) Single-channel decovnoltuion results for SNR=0 dB. (b) Single-channel decovnoltuion results for SNR=5 dB. (c) MC I results for SNR=0 dB. (d) MC I results for SNR=5 dB. (e) MC II results for SNR=0 dB. (f) MC II results for SNR=5 dB.

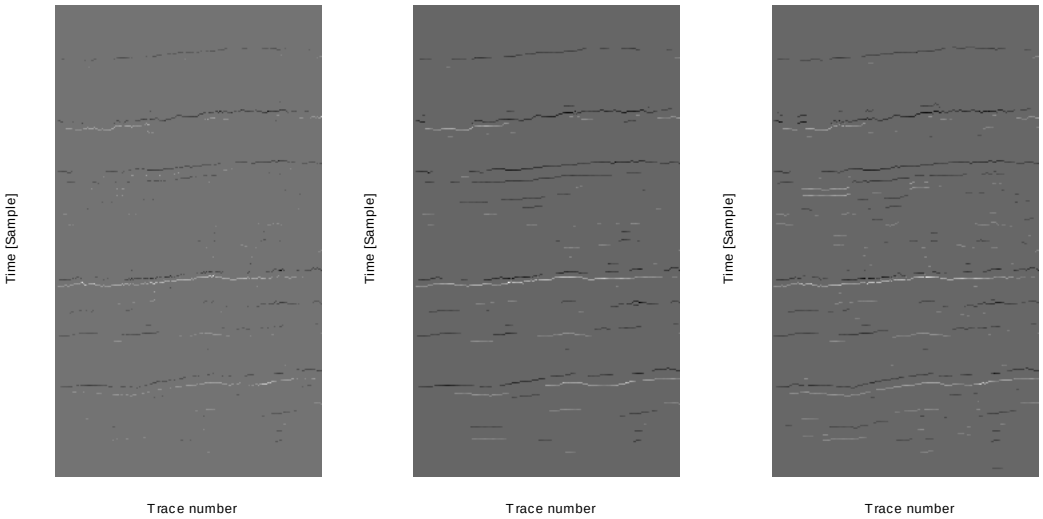

(a) (b) (c)

Figure 4.4: Real data MC II results: (a) Single-channel deconvolution results. (b) MC I results. (c) MC II results.

Chapter 5

Conclusion

5.1 Summary

We have proposed two multichannel blind deconvolution algorithms. Both algorithms are based on the MBG I reflectivity model and carry out the deconvolution iteratively.

The first proposed algorithm employs in each iteration a modified MPM algorithm which estimates the current reflectivity column from the corresponding observed trace and an estimate of the preceding reflectivity column. The second proposed algorithm employs in each iteration a further modified MPM algorithm which takes into account estimates of both the preceding and subsequent columns in the estimation process of the current reflectivity column. Both algorithms, which take into account the spatial dependency between neighboring traces in the deconvolution process, showed better performance than a single-channel deconvolution algorithm, for synthetic and real data. The second algorithm uses more

information from neighboring traces in the deconvolution process of each trace, and therefore performs better than the first proposed algorithm, on synthetic and real data.

5.2 Future Research

The methods we have proposed in this thesis open a number of interesting topics for future study:

1. Both proposed algorithms use the MBG I reflectivity prior model. Idier and Goussard also propose in [15] the MBG II model, which uses a different amplitude field than the MBG I model. Developing new versions of the two proposed algorithm which are based on the MBG II model may lead to different quality of the deconvolution results. The performance of the new algorithms can be assessed and compared to that of the original ones.

2. The deconvolution scheme of the second proposed algorithm uses the second proposed window type which has a size of two columns. Increasing the window size will incorporate more information from subsequent columns in the estimation process of the jth reflectivity column, which may lead to better deconvolution results (at the cost of higher computational complexity). It is also interesting to check whether for larger windows sizes, deconvolution results obtained using the first type of estimation window are still inferior to those obtained by the second type.

3. The proposed parameter estimation method assumes that the wavelet's

length and maximum position are known. Estimating the missing parameters using algorithms such as the one proposed by Labat and Idier [26], which do not require the maximum position of the wavelet, or the one proposed by Nsiri et al. [27], which is able to estimate the wavelet's length and maximum position, may lead to a more robust blind deconvolution scheme.

4. The second proposed algorithm can be expanded to handle 3D input data. In this case the recovered reflectivity is also a 3D signal and a 3D estimation window can be used so that neighboring reflectivity columns from 4 directions will be taken into account in the estimation process of each reflectivity column.

Appendix A

Derivation Of Conditional distributions

A.1 Derivation of the parameters $\lambda_{k,j}^b, m_{k,j}^b$ and $V_{k,j}^b$

Our goal is to derive the BG distribution $p\left(r_{k,j}, q_{k,j} \left| \mathbf{y}_j, \mathbf{r}_{-k,j}, \mathbf{q}_{-k,j}, \mathbf{t}_{j-1}^{/}, \mathbf{t}_{j-1}^{-}, \mathbf{t}_{j-1}^{\backslash}, \mathbf{r}_{j-1} \right.\right)$. We start by factoring this distribution as:

$$\begin{aligned} & p\left(r_{k,j}, q_{k,j} \left| \mathbf{y}_j, \mathbf{r}_{-k,j}, \mathbf{q}_{-k,j}, \mathbf{t}_{j-1}^{/}, \mathbf{t}_{j-1}^{-}, \mathbf{t}_{j-1}^{\backslash}, \mathbf{r}_{j-1} \right.\right) \\ & \propto p\left(\mathbf{y}_j \left| \mathbf{r}_j \right.\right) p\left(r_{k,j} \left| q_{k,j}, \mathbf{t}_{j-1}^{/}, \mathbf{t}_{j-1}^{-}, \mathbf{t}_{j-1}^{\backslash}, \mathbf{r}_{j-1} \right.\right) p\left(q_{k,j} \left| \mathbf{t}_{k+1,j-1}^{/}, \mathbf{t}_{k,j-1}^{-}, \mathbf{t}_{k-1,j-1}^{\backslash} \right.\right). \end{aligned} \tag{A.1}$$

Noting that

$$p\left(q_{k,j}\left|\mathbf{t}^{/}_{k+1,j-1},\mathbf{t}^{-}_{k,j-1},\mathbf{t}^{\backslash}_{k-1,j-1}\right.\right)\sim B\left(\lambda^{t}_{k,j}\right) \tag{A.2}$$

with $\lambda^{t}_{k,j}=\varepsilon^{\left(1-\mathbf{t}^{/}_{k+1,j-1}\right)\left(1-\mathbf{t}^{-}_{k,j-1}\right)\left(1-\mathbf{t}^{\backslash}_{k-1,j-1}\right)}$, and defining

$$p\left(r_{k,j}\left|q_{k,j}=1,\mathbf{t}^{/}_{j-1},\mathbf{t}^{-}_{j-1},\mathbf{t}^{\backslash}_{j-1},\mathbf{r}_{j-1}\right.\right)\sim N\left(m_{k,j},\sigma^{2}_{k,j}\right) \tag{A.3}$$

we get, after some algebraic manipulations:

$$\begin{aligned}&p\left(r_{k,j},q_{k,j}=1\left|\mathbf{y}_{j},\mathbf{r}_{-k,j},\mathbf{q}_{-k,j},\mathbf{t}^{/}_{j-1},\mathbf{t}^{-}_{j-1},\mathbf{t}^{\backslash}_{j-1},\mathbf{r}_{j-1}\right.\right)\\&\propto\lambda^{t}_{k,j}\frac{\sqrt{V^{b}_{k,j}}}{\sigma_{k,j}}\exp\left[-\frac{m^{2}_{k,j}}{2\sigma^{2}_{k,j}}+\frac{\left(m^{b}_{k,j}\right)^{2}}{2V^{b}_{k,j}}\right]\frac{1}{\sqrt{2\pi V^{b}_{k,j}}}\exp\left[-\frac{\left(r_{k,j}-m^{b}_{k,j}\right)^{2}}{2V^{b}_{k,j}}\right]\end{aligned} \tag{A.4}$$

with $V^{b}_{k,j}=\left(\frac{1}{\sigma^{2}_{k,j}}+\frac{1}{V_{w}}\right)^{-1}$, $m^{b}_{k,j}=V^{b}_{k,j}\left(\frac{m_{k,j}}{\sigma^{2}_{k,j}}+\frac{m_{w}}{V_{w}}\right)$, $V_{w}=\frac{\sigma^{2}_{w}}{E_{h}}$,
$m_{w}=\frac{1}{E_{h}}\sum_{i=1}^{N_{h}}h(i)\left[y_{k+i-1,j}-\sum_{\substack{s=1\\s\neq i}}^{N_{h}}h(s)r_{i+k-s,j}\right]$, $E_{h}=\sum_{i=1}^{N_{h}}h^{2}(i)$.

Similarly, we get that

$$p\left(r_{k,j},q_{k,j}=0\left|\mathbf{y}_{j},\mathbf{r}_{-k,j},\mathbf{q}_{-k,j},\mathbf{t}^{/}_{j-1},\mathbf{t}^{-}_{j-1},\mathbf{t}^{\backslash}_{j-1},\mathbf{r}_{j-1}\right.\right)\propto\left(1-\lambda^{t}_{k,j}\right)\delta\left(r_{k,j}\right). \tag{A.5}$$

Finally, from (A.4) and (A.5) we get that

$$p\left(q_{k,j}\left|\mathbf{y}_{j},\mathbf{r}_{-k,j},\mathbf{q}_{-k,j},\mathbf{t}^{/}_{j-1},\mathbf{t}^{-}_{j-1},\mathbf{t}^{\backslash}_{j-1},\mathbf{r}_{j-1}\right.\right)\sim B\left(\lambda^{b}_{k,j}\right) \tag{A.6}$$

and

$$p\left(r_{k,j}, q_{k,j} \left| \mathbf{y}_j, \mathbf{r}_{-k,j}, \mathbf{q}_{-k,j}, \mathbf{t}^{/}_{j-1}, \mathbf{t}^{-}_{j-1}, \mathbf{t}^{\backslash}_{j-1}, \mathbf{r}_{j-1}\right.\right) \sim \lambda^b_{k,j} N\left(m^b_{k,j}, V^b_{k,j}\right) + \left(1-\lambda^b_{k,j}\right)\delta\left(r_{k,j}\right) \tag{A.7}$$

where

$$\begin{aligned}\lambda^b_{k,j} &= p\left(q_{k,j}=1 \left| \mathbf{y}_j, \mathbf{r}_{-k,j}, \mathbf{q}_{-k,j}, \mathbf{t}^{/}_{j-1}, \mathbf{t}^{-}_{j-1}, \mathbf{t}^{\backslash}_{j-1}, \mathbf{r}_{j-1}\right.\right) \\ &= \left\{1 + \frac{1-\lambda^t_{k,j}}{\lambda^t_{k,j}} \frac{\sigma_{k,j}}{\sqrt{V^b_{k,j}}} \exp\left[-\frac{(m^b_{k,j})^2}{2V^b_{k,j}} + \frac{m^2_{k,j}}{2\sigma^2_{k,j}}\right]\right\}^{-1}. \end{aligned} \tag{A.8}$$

A.2 Derivation of the parameters $\mu^{/}_{k,j-1}, \mu^{-}_{k,j-1}$ and $\mu^{\backslash}_{k,j-1}$

We will now derive the conditional probabilities for the three types of transition variables. Let $S_{k,j} = \{-1 \leq dk \leq 1 : q_{k+dk,j} = 1\}$, then we start with $p\left(t^{/}_{k,j-1} \left| \mathbf{r}_j, \mathbf{q}_j, \mathbf{t}^{/}_{-k,j-1}, \mathbf{t}^{-}_{j-1}, \mathbf{t}^{\backslash}_{j-1}, \mathbf{r}_{j-1}, \mathbf{q}_{j-1}\right.\right)$, which can be expressed by

$$\begin{aligned} & p\left(t^{/}_{k,j-1} \left| \mathbf{r}_j, \mathbf{q}_j, \mathbf{t}^{/}_{-k,j-1}, \mathbf{t}^{-}_{j-1}, \mathbf{t}^{\backslash}_{j-1}, \mathbf{r}_{j-1}, \mathbf{q}_{j-1}\right.\right) \\ & \propto p\left(q_{k-1,j} \left| \mathbf{t}^{/}_{k,j-1}, \mathbf{t}^{-}_{k-1,j-1}, \mathbf{t}^{\backslash}_{k-2,j-1}\right.\right) p\left(\mathbf{t}^{/}_{k,j-1}, \mathbf{t}^{-}_{k,j-1}, \mathbf{t}^{\backslash}_{k,j-1} \left| q_{k,j-1}\right.\right) \\ & \times \prod_{dk \in S_{k,j}} p\left(r_{k+dk,j} \left| q_{k+dk,j}, \mathbf{t}^{/}_{j-1}, \mathbf{t}^{-}_{j-1}, \mathbf{t}^{\backslash}_{j-1}, \mathbf{r}_{j-1}\right.\right). \end{aligned} \tag{A.9}$$

We first note that $p\left(t^{/}_{k,j-1}=1 \left| \mathbf{r}_j, \mathbf{q}_j, \mathbf{t}^{/}_{-k,j-1}, \mathbf{t}^{-}_{j-1}, \mathbf{t}^{\backslash}_{j-1}, \mathbf{r}_{j-1}, \mathbf{q}_{j-1}\right.\right) \neq 0$ only when $q_{k,j-1}=1$ and $q_{k-1,j}=1$. We also note that using Bayes rule and some algebraic

manipulations we can write:

$$
\begin{aligned}
& p\left(t^{/}_{k,j-1}, t^{-}_{k,j-1}, t^{\backslash}_{k,j-1} \,|q_{k,j-1}=1\right) \\
= & \left[\frac{\left(\mu^{/}\right)^{t^{/}_{k,j-1}}\left(1-\mu^{/}\right)^{1-t^{/}_{k,j-1}}\left(\mu^{-}\right)^{t^{-}_{k,j-1}}\left(1-\mu^{-}\right)^{1-t^{-}_{k,j-1}}\left(\mu^{\backslash}\right)^{t^{\backslash}_{k,j-1}}\left(1-\mu^{\backslash}\right)^{1-t^{\backslash}_{k,j-1}}}{\lambda}\right. \\
& \left.-\frac{(1-\lambda)\binom{1-t^{/}_{k,j-1}}{}\binom{1-t^{-}_{k,j-1}}{}\binom{1-t^{\backslash}_{k,j-1}}{}}{\lambda}\right]
\end{aligned}
\tag{A.10}
$$

Next, let

$$\rho^{/}_{1,dk} = p\left(r_{k+dk,j}\,\middle|q_{k+dk,j}, \mathbf{t}^{/}_{k,j-1}=1, \mathbf{t}^{/}_{-k,j-1}, \mathbf{t}^{-}_{j-1}, \mathbf{t}^{\backslash}_{j-1}, \mathbf{r}_{j-1}\right) \tag{A.11}$$

$$\rho^{/}_{0,dk} = p\left(r_{k+dk,j}\,\middle|q_{k+dk,j}, \mathbf{t}^{/}_{k,j-1}=0, \mathbf{t}^{/}_{-k,j-1}, \mathbf{t}^{-}_{j-1}, \mathbf{t}^{\backslash}_{j-1}, \mathbf{r}_{j-1}\right) \tag{A.12}$$

$$\eta^{/}_{1} = p\left(\mathbf{t}^{/}_{k,j-1}=1, \mathbf{t}^{-}_{k,j-1}, \mathbf{t}^{\backslash}_{k,j-1} \,|q_{k,j-1}=1\right) \tag{A.13}$$

$$\eta^{/}_{0} = p\left(q_{k-1,j}=1\,\middle|\mathbf{t}^{/}_{k,j-1}=0, \mathbf{t}^{-}_{k-1,j-1}, \mathbf{t}^{\backslash}_{k-2,j-1}\right) p\left(\mathbf{t}^{/}_{k,j-1}=0, \mathbf{t}^{-}_{k,j-1}, \mathbf{t}^{\backslash}_{k,j-1} \,|q_{k,j-1}=1\right) \tag{A.14}$$

Then using (A.9), (A.11) and (A.13) we get:

$$
\begin{aligned}
& p\left(\mathbf{t}^{/}_{k,j-1}=1\,\middle|\mathbf{r}_{j}, q_{k-1,j}=1, \mathbf{q}_{-(k-1),j}, \mathbf{t}^{/}_{-k,j-1}, \mathbf{t}^{-}_{j-1}, \mathbf{t}^{\backslash}_{j-1}, \mathbf{r}_{j-1}, q_{k,j-1}=1, \mathbf{q}_{-k,j-1}\right) \\
& \propto \eta^{/}_{1} \prod_{dk\in S_{k,j}} \rho^{/}_{1,dk}
\end{aligned}
\tag{A.15}
$$

and using (A.9), (A.12) and (A.14) we get:

$$p\left(\mathbf{t}^{/}_{k,j-1}=0\,\middle|\,\mathbf{r}_{,j},q_{k-1,j}=1,\mathbf{q}_{-(k-1),j},\mathbf{t}^{/}_{-k,j-1},\mathbf{t}^{-}_{j-1},\mathbf{t}^{\backslash}_{j-1},\mathbf{r}_{j-1},q_{k,j-1}=1,\mathbf{q}_{-k,j-1}\right)$$
$$\propto \eta^{/}_{0}\prod_{dk\in S_{k,j}}\rho^{/}_{0,dk} \tag{A.16}$$

Now, from (A.15) and (A.16) we get that

$$p\left(t^{/}_{k,j-1}\,\middle|\,\mathbf{r}_{j},\mathbf{q}_{j},\mathbf{t}^{/}_{-k,j-1},\mathbf{t}^{-}_{j-1},\mathbf{t}^{\backslash}_{j-1},\mathbf{r}_{j-1},\mathbf{q}_{j-1}\right)\sim B\left(\mu^{/}_{k,j-1}\right) \tag{A.17}$$

with

$$\begin{aligned}\mu^{/}_{k,j-1}&=p\left(t^{/}_{k,j-1}=1\,\middle|\,\mathbf{r}_{j},\mathbf{q}_{j},\mathbf{t}^{/}_{-k,j-1},\mathbf{t}^{-}_{j-1},\mathbf{t}^{\backslash}_{j-1},\mathbf{r}_{j-1},\mathbf{q}_{j-1}\right)\\&=\begin{cases}\left(1+\frac{\eta^{/}_{0}}{\eta^{/}_{1}}\prod_{dk\in S_{k,j}}\frac{\rho^{/}_{0,dk}}{\rho^{/}_{1,dk}}\right)^{-1}, & \text{if } q_{k-1,j}=q_{k,j-1}=1\\ 0, & \text{otherwise}\end{cases}\end{aligned} \tag{A.18}$$

Similarly, let

$$\rho^{-}_{1,dk}=p\left(r_{k+dk,j}\,\middle|\,q_{k+dk,j},\mathbf{t}^{-}_{k,j-1}=0,\mathbf{t}^{/}_{j-1},\mathbf{t}^{-}_{-k,j-1},\mathbf{t}^{\backslash}_{j-1},\mathbf{r}_{j-1}\right) \tag{A.19}$$

$$\rho^{-}_{0,dk}=p\left(r_{k+dk,j}\,\middle|\,q_{k+dk,j},\mathbf{t}^{-}_{k,j-1}=1,\mathbf{t}^{/}_{j-1},\mathbf{t}^{-}_{-k,j-1},\mathbf{t}^{\backslash}_{j-1},\mathbf{r}_{j-1}\right) \tag{A.20}$$

$$\eta^{-}_{1}=p\left(\mathbf{t}^{/}_{k,j-1},\mathbf{t}^{-}_{k,j-1}=1,\mathbf{t}^{\backslash}_{k,j-1}\,|q_{k,j-1}=1\right) \tag{A.21}$$

$$\eta^{-}_{0}=p\left(q_{k,j}=1\,\middle|\,\mathbf{t}^{/}_{k+1,j-1},\mathbf{t}^{-}_{k,j-1}=0,\mathbf{t}^{\backslash}_{k-1,j-1}\right)p\left(\mathbf{t}^{/}_{k,j-1},\mathbf{t}^{-}_{k,j-1}=0,\mathbf{t}^{\backslash}_{k,j-1}\,|q_{k,j-1}=1\right). \tag{A.22}$$

Then it can be shown that:

$$p\left(t^{-}_{k,j-1}\left|\mathbf{r}_j,\mathbf{q}_j,\mathbf{t}^{/}_{j-1},\mathbf{t}^{-}_{-k,j-1},\mathbf{t}^{\backslash}_{j-1},\mathbf{r}_{j-1},\mathbf{q}_{j-1}\right.\right)\sim B\left(\mu^{-}_{k,j-1}\right) \tag{A.23}$$

with

$$\begin{aligned}\mu^{-}_{k,j-1} &= p\left(t^{-}_{k,j-1}=1\left|\mathbf{r}_j,\mathbf{q}_j,\mathbf{t}^{/}_{j-1},\mathbf{t}^{-}_{-k,j-1},\mathbf{t}^{\backslash}_{j-1},\mathbf{r}_{j-1},\mathbf{q}_{j-1}\right.\right)\\ &= \begin{cases}\left(1+\frac{\eta^{-}_{0}}{\eta^{-}_{1}}\prod\limits_{dk\in S_{k,j}}\frac{\rho^{-}_{0,dk}}{\rho^{-}_{1,dk}}\right)^{-1} & \text{if } q_{k,j}=q_{k,j-1}=1\\ 0 & \text{else}\end{cases}\end{aligned} \tag{A.24}$$

Finally, let

$$\rho^{\backslash}_{1,dk} = p\left(r_{k+dk,j}\left|q_{k+dk,j},\mathbf{t}^{\backslash}_{k,j-1}=0,\mathbf{t}^{/}_{j-1},\mathbf{t}^{-}_{j-1},\mathbf{t}^{\backslash}_{-k,j-1},\mathbf{r}_{j-1}\right.\right) \tag{A.25}$$

$$\rho^{\backslash}_{0,dk} = p\left(r_{k+dk,j}\left|q_{k+dk,j},\mathbf{t}^{\backslash}_{k,j-1}=1,\mathbf{t}^{/}_{j-1},\mathbf{t}^{-}_{j-1},\mathbf{t}^{\backslash}_{-k,j-1},\mathbf{r}_{j-1}\right.\right) \tag{A.26}$$

$$\eta^{\backslash}_{1} = p\left(\mathbf{t}^{/}_{k,j-1},\mathbf{t}^{-}_{k,j-1},\mathbf{t}^{\backslash}_{k,j-1}=1\left|q_{k,j-1}=1\right.\right) \tag{A.27}$$

$$\eta^{\backslash}_{0} = p\left(q_{k+1,j}=1\left|\mathbf{t}^{/}_{k+2,j-1},\mathbf{t}^{-}_{k+1,j-1},\mathbf{t}^{\backslash}_{k,j-1}=0\right.\right)p\left(\mathbf{t}^{/}_{k,j-1},\mathbf{t}^{-}_{k,j-1},\mathbf{t}^{\backslash}_{k,j-1}=0\left|q_{k,j-1}=1\right.\right). \tag{A.28}$$

Then,

$$p\left(t^{\backslash}_{k,j-1}\left|\mathbf{r}_j,\mathbf{q}_j,\mathbf{t}^{/}_{,j-1},\mathbf{t}^{-}_{j-1},\mathbf{t}^{\backslash}_{-k,j-1},\mathbf{r}_{j-1},\mathbf{q}_{j-1}\right.\right)\sim B\left(\mu^{\backslash}_{k,j-1}\right) \tag{A.29}$$

with

$$\begin{aligned}\mu^{\backslash}_{k,j-1} &= p\left(t^{\backslash}_{k,j-1}=1\,\middle|\,\mathbf{r}_j,\mathbf{q}_j,\mathbf{t}^{/}_{,j-1},\mathbf{t}^{-}_{j-1},\mathbf{t}^{\backslash}_{-k,j-1},\mathbf{r}_{j-1},\mathbf{q}_{j-1}\right)\\ &= \begin{cases}\left(1+\frac{\eta^{\backslash}_0}{\eta^{\backslash}_1}\prod\limits_{dk\in S_{k,j}}\frac{\rho^{\backslash}_{0,dk}}{\rho^{\backslash}_{1,dk}}\right)^{-1} & \text{if } q_{k+1,j}=q_{k,j-1}=1\\ 0 & \text{else}\end{cases}\end{aligned} \tag{A.30}$$

A.3 Derivation of the parameters $\lambda^f_{k,j}, m^f_{k,j}$ and $V^f_{k,j}$

Our goal is to derive the BG distribution $p\left(r_{k,j},q_{k,j}\,\middle|\,\mathbf{y}_j,\mathbf{r}_{-k,j},\mathbf{q}_{-k,j},\mathbf{r}_{j+1},\mathbf{q}_{j+1},\mathbf{t}^{/}_j,\mathbf{t}^{-}_j,\mathbf{t}^{\backslash}_j\right)$. Let $S_{k,j+1} = \{-1\le dk\le 1 : q_{k+dk,j+1}=1\}$, then this distribution can be rewritten as:

$$\begin{aligned}&p\left(r_{k,j},q_{k,j}\,\middle|\,\mathbf{y}_j,\mathbf{r}_{-k,j},\mathbf{q}_{-k,j},\mathbf{r}_{j+1},\mathbf{q}_{j+1},\mathbf{t}^{/}_j,\mathbf{t}^{-}_j,\mathbf{t}^{\backslash}_j\right)\\ &\propto p\left(\mathbf{y}_j\,|\mathbf{r}_j\right)p\left(t^{/}_{k,j},t^{-}_{k,j},t^{\backslash}_{k,j}\,|q_{k,j}\right)p\left(r_{k,j}\,|q_{k,j}\right)p\left(q_{k,j}\right)\\ &\times\prod_{dk\in S_{k,j+1}}p\left(r_{k+dk,j+1}\,\middle|\,q_{k+dk,j+1},\mathbf{t}^{/}_j,\mathbf{t}^{-}_j,\mathbf{t}^{\backslash}_j,\mathbf{r}_j\right).\end{aligned} \tag{A.31}$$

Noticing that

$$p\left(r_{k+dk,j+1}\,\middle|\,q_{k+dk,j+1}=1,\mathbf{t}^{/}_j,\mathbf{t}^{-}_j,\mathbf{t}^{\backslash}_j,\mathbf{r}_j\right)\sim N\left(m_{k+dk,j+1},\sigma^2_{k+dk,j+1}\right) \tag{A.32}$$

and defining

$$g_1 = p\left(t^{/}_{k,j},t^{-}_{k,j},t^{\backslash}_{k,j}\,|q_{k,j}=1\right)p\left(q_{k,j}=1\right) \tag{A.33}$$

and

$$a_{dk} = \begin{cases} a & \text{if } r_{k+dk,j+1} \text{ and } r_{k,j} \text{ are correlated} \\ 0 & \text{otherwise} \end{cases} \tag{A.34}$$

we get that

$$\begin{aligned} & p\left(r_{k,j}, q_{k,j} = 1 \left| \mathbf{y}_j, \mathbf{r}_{-k,j}, \mathbf{q}_{-k,j}, \mathbf{r}_{j+1}, \mathbf{q}_{j+1}, \mathbf{t}_j^{/}, \mathbf{t}_j^{-}, \mathbf{t}_j^{\backslash}\right.\right) \\ & \propto \frac{\sqrt{V_{k,j}^f} g_1}{\sigma_r} \exp\left[\frac{(m_{k,j}^f)^2}{2V_{k,j}^f}\right] \frac{1}{\sqrt{2\pi V_{k,j}^f}} \exp\left[-\frac{\left(r_{k,j} - m_{k,j}^f\right)^2}{2V_{k,j}^f}\right] \\ & \times \prod_{dk \in S_{k,j+1}} \frac{1}{\sqrt{2\pi\left(1 - a_{dk}^2\right)\sigma_r^2}} \exp\left[-\frac{r_{k+dk,j+1}^2}{2\left(1 - a_{dk}^2\right)\sigma_r^2}\right] \end{aligned} \tag{A.35}$$

with $V_{k,j}^f = \left[\frac{1}{\sigma_r^2} + \frac{1}{V_w} + \sum_{dk \in S_{k,j+1}} \frac{a_{dk}^2}{\left(1-a_{dk}^2\right)\sigma_r^2}\right]^{-1}$, $m_{k,j}^f = V_{k,j}^f \left[\sum_{dk \in S_{k,j+1}} \frac{a_{dk} r_{k+dk,j+1}}{\left(1-a_{dk}^2\right)\sigma_r^2} + \frac{m_w}{V_w}\right]$,

$V_w = \frac{\sigma_w^2}{E_h}$, $m_w = \frac{1}{E_h} \sum_{i=1}^{N_h} h(i) \left[y_{k+i-1,j} - \sum_{\substack{s=1 \\ s \neq i}}^{N_h} h(s) r_{i+k-s,j}\right]$, $E_h = \sum_{i=1}^{N_h} h^2(i)$.

Similarly, let

$$g_0 = p\left(t_{k,j}^{/}, t_{k,j}^{-}, t_{k,j}^{\backslash} \left| q_{k,j} = 0\right.\right) p\left(q_{k,j} = 0\right) \tag{A.36}$$

then

$$\begin{aligned} & p\left(r_{k,j}, q_{k,j} = 0 \left| \mathbf{y}_j, \mathbf{r}_{-k,j}, \mathbf{q}_{-k,j}, \mathbf{r}_{j+1}, \mathbf{q}_{j+1}, \mathbf{t}_j^{/}, \mathbf{t}_j^{-}, \mathbf{t}_j^{\backslash}\right.\right) \\ & \propto g_0 \delta\left(r_{k,j}\right) \prod_{dk \in S_{k,j+1}} \frac{1}{\sqrt{2\pi\sigma_r^2}} \exp\left(-\frac{r_{k+dk,j+1}^2}{2\sigma_r^2}\right) \end{aligned} \tag{A.37}$$

Finally, from (A.35) and (A.37) we get that

$$p\left(q_{k,j}\left|\mathbf{y}_j,\mathbf{r}_{-k,j},\mathbf{q}_{-k,j},\mathbf{r}_{j+1},\mathbf{q}_{j+1},\mathbf{t}'_j,\mathbf{t}^-_j,\mathbf{t}^{\backslash}_j\right.\right)\sim Be\left(\lambda^f_{k,j}\right) \tag{A.38}$$

$$p\left(r_{k,j},q_{k,j}\left|\mathbf{y}_j,\mathbf{r}_{-k,j},\mathbf{q}_{-k,j},\mathbf{r}_{j+1},\mathbf{q}_{j+1},\mathbf{t}'_j,\mathbf{t}^-_j,\mathbf{t}^{\backslash}_j\right.\right)\sim\lambda^f_{k,j}N\left(m^f_{k,j},V^f_{k,j}\right)+\left(1-\lambda^f_{k,j}\right)\delta\left(r_{k,j}\right) \tag{A.39}$$

where

$$\begin{aligned}\lambda^f_{k,j}&=p\left(q_{k,j}=1\left|\mathbf{y}_j,\mathbf{r}_{-k,j},\mathbf{q}_{-k,j},\mathbf{r}_{j+1},\mathbf{q}_{j+1},\mathbf{t}'_j,\mathbf{t}^-_j,\mathbf{t}^{\backslash}_j\right.\right)\\&=\left\{1+\frac{\sigma_r g_0}{\sqrt{V^f_{k,j}}g_1}\exp\left[-\frac{(m^f_{k,j})^2}{2V^f_{k,j}}-\sum_{dk\in S_{k,j+1}}\frac{a^2_{dk}r^2_{k+dk,j+1}}{2\left(1-a^2_{dk}\right)\sigma^2_r}\right]\prod_{dk\in S_{k,j+1}}\sqrt{1-a^2_{dk}}\right\}^{-1}.\end{aligned} \tag{A.40}$$

A.4 Derivation of the parameters $\lambda_{k,j}^m, m_{k,j}^m$ and $V_{k,j}^m$

The BG distribution $p\left(r_{k,j}, q_{k,j} \left| \mathbf{y}_j, \mathbf{r}_{-k,j}, \mathbf{q}_{-k,j}, \mathbf{t}_{j-1}^{/}, \mathbf{t}_{j-1}^{-}, \mathbf{t}_{j-1}^{\backslash}, \mathbf{r}_{j-1}, \mathbf{r}_{j+1}, \mathbf{q}_{j+1}, \mathbf{t}_{j}^{/}, \mathbf{t}_{j}^{-}, \mathbf{t}_{j}^{\backslash}\right.\right)$ can be rewritten as:

$$\begin{aligned}
&p\left(r_{k,j}, q_{k,j} \left| \mathbf{y}_j, \mathbf{r}_{-k,j}, \mathbf{q}_{-k,j}, \mathbf{t}_{j-1}^{/}, \mathbf{t}_{j-1}^{-}, \mathbf{t}_{j-1}^{\backslash}, \mathbf{r}_{j-1}, \mathbf{r}_{j+1}, \mathbf{q}_{j+1}, \mathbf{t}_{j}^{/}, \mathbf{t}_{j}^{-}, \mathbf{t}_{j}^{\backslash}\right.\right) \\
&\propto p\left(\mathbf{y}_j \left| \mathbf{r}_j \right.\right) p\left(t_{k,j}^{/}, t_{k,j}^{-}, t_{k,j}^{\backslash} \left| q_{k,j} \right.\right) p\left(r_{k,j} \left| q_{k,j}, \mathbf{t}_{j-1}^{/}, \mathbf{t}_{j-1}^{-}, \mathbf{t}_{j-1}^{\backslash}, \mathbf{r}_{j-1} \right.\right) \\
&\times p\left(q_{k,j} \left| \mathbf{t}_{k+1,j-1}^{/}, \mathbf{t}_{k,j-1}^{-}, \mathbf{t}_{k-1,j-1}^{\backslash} \right.\right) \prod_{dk \in S_{k,j+1}} p\left(r_{k+dk,j+1} \left| q_{k+dk,j+1}, \mathbf{t}_{j}^{/}, \mathbf{t}_{j}^{-}, \mathbf{t}_{j}^{\backslash}, \mathbf{r}_j \right.\right).
\end{aligned} \tag{A.41}$$

Let

$$c_1 = p\left(t_{k,j}^{/}, t_{k,j}^{-}, t_{k,j}^{\backslash} \left| q_{k,j} = 1 \right.\right) p\left(q_{k,j} = 1 \left| \mathbf{t}_{k+1,j-1}^{/}, \mathbf{t}_{k,j-1}^{-}, \mathbf{t}_{k-1,j-1}^{\backslash} \right.\right) \tag{A.42}$$

then using (A.3), (A.32) and (A.34) we get that

$$\begin{aligned}
&p\left(r_{k,j}, q_{k,j} = 1 \left| \mathbf{y}_j, \mathbf{r}_{-k,j}, \mathbf{q}_{-k,j}, \mathbf{t}_{j-1}^{/}, \mathbf{t}_{j-1}^{-}, \mathbf{t}_{j-1}^{\backslash}, \mathbf{r}_{j-1}, \mathbf{r}_{j+1}, \mathbf{q}_{j+1}, \mathbf{t}_{j}^{/}, \mathbf{t}_{j}^{-}, \mathbf{t}_{j}^{\backslash}\right.\right) \\
&\propto \frac{\sqrt{V_{k,j}^m} c_1}{\sigma_{k,j}} \exp\left[-\frac{m_{k,j}^2}{2\sigma_{k,j}^2} + \frac{(m_{k,j}^m)^2}{2V_{k,j}^m}\right] \frac{1}{\sqrt{2\pi V_{k,j}^m}} \exp\left[-\frac{\left(r_{k,j} - m_{k,j}^m\right)^2}{2V_{k,j}^m}\right] \\
&\times \prod_{dk \in S_{k,j+1}} \frac{1}{\sqrt{2\pi\left(1 - a_{dk}^2\right)\sigma_r^2}} \exp\left[-\frac{r_{k+dk,j+1}^2}{2\left(1 - a_{dk}^2\right)\sigma_r^2}\right]
\end{aligned} \tag{A.43}$$

with $V_{k,j}^m = \left[\frac{1}{\sigma_{k,j}^2} + \frac{1}{V_w}\sum_{dk\in S_{k,j+1}} \frac{\tilde{a}_{dk}^2 \mathbf{q}_{k+dk,j+1}}{\left(1-\tilde{a}_{dk}^2\right)\sigma_r^2}\right]^{-1}$, $m_{k,j}^m = V_{k,j}^m \left[\sum_{dk\in S_{k,j+1}} \frac{\tilde{a}_{dk} r_{k+dk,j+1}}{\left(1-\tilde{a}_{dk}^2\right)\sigma_r^2} + \frac{m_{k,j}}{\sigma_{k,j}^2} + \frac{m_w}{V_w}\right]$

$V_w = \frac{\sigma_w^2}{E_h}$, $m_w = \frac{1}{E_h}\sum_{i=1}^{N_h} h(i)\left[y_{k+i-1,j} - \sum_{\substack{s=1\\ s\neq i}}^{N_h} h(s) r_{i+k-s,j}\right]$, $E_h = \sum_{i=0}^{L} h^2(i)$.

Similarly, let

$$c_0 = p\left(t_{k,j}^{/}, t_{k,j}^{-}, t_{k,j}^{\backslash} \,|q_{k,j}=0\right) p\left(q_{k,j}=0 \,\middle|\, \mathbf{t}_{k+1,j-1}^{/}, \mathbf{t}_{k,j-1}^{-}, \mathbf{t}_{k-1,j-1}^{\backslash}\right) \tag{A.44}$$

then

$$\begin{aligned} &p\left(r_{k,j}, q_{k,j}=0 \,\middle|\, \mathbf{y}_j, \mathbf{r}_{-k,j}, \mathbf{q}_{-k,j}, \mathbf{t}_{j-1}^{/}, \mathbf{t}_{j-1}^{-}, \mathbf{t}_{j-1}^{\backslash}, \mathbf{r}_{j-1}, \mathbf{r}_{j+1}, \mathbf{q}_{j+1}, \mathbf{t}_j^{/}, \mathbf{t}_j^{-}, \mathbf{t}_j^{\backslash}\right) \\ &\propto c_0 \delta\left(r_{k,j}\right) \prod_{dk\in S_{k,j+1}} \frac{1}{\sqrt{2\pi\sigma_r^2}} \exp\left(-\frac{r_{k+dk,j+1}^2}{2\sigma_r^2}\right) \end{aligned} \tag{A.45}$$

Finally, from (A.43) and (A.45) we get that

$$p\left(q_{k,j} \,\middle|\, \mathbf{y}_j, \mathbf{r}_{-k,j}, \mathbf{q}_{-k,j}, \mathbf{t}_{j-1}^{/}, \mathbf{t}_{j-1}^{-}, \mathbf{t}_{j-1}^{\backslash}, \mathbf{r}_{j-1}, \mathbf{r}_{j+1}, \mathbf{q}_{j+1}, \mathbf{t}_j^{/}, \mathbf{t}_j^{-}, \mathbf{t}_j^{\backslash}\right) \sim B\left(\lambda_{k,j}^m\right) \tag{A.46}$$

$$\begin{aligned} &p\left(r_{k,j}, q_{k,j} \,\middle|\, \mathbf{y}_j, \mathbf{r}_{-k,j}, \mathbf{q}_{-k,j}, \mathbf{t}_{j-1}^{/}, \mathbf{t}_{j-1}^{-}, \mathbf{t}_{j-1}^{\backslash}, \mathbf{r}_{j-1}, \mathbf{r}_{j+1}, \mathbf{q}_{j+1}, \mathbf{t}_j^{/}, \mathbf{t}_j^{-}, \mathbf{t}_j^{\backslash}\right) \\ &\sim \lambda_{k,j}^m N\left(m_{k,j}^m, V_{k,j}^m\right) + \left(1-\lambda_{k,j}^m\right)\delta\left(r_{k,j}\right) \end{aligned} \tag{A.47}$$

where

$$\begin{aligned}\lambda_{k,j}^{m} &= p\left(q_{k,j}=1 \,\middle|\, \mathbf{y}_j, \mathbf{r}_{-k,j}, \mathbf{q}_{-k,j}, \mathbf{t}_{j-1}^{/}, \mathbf{t}_{j-1}^{-}, \mathbf{t}_{j-1}^{\backslash}, \mathbf{r}_{j-1}, \mathbf{r}_{j+1}, \mathbf{q}_{j+1}, \mathbf{t}_{j}^{/}, \mathbf{t}_{j}^{-}, \mathbf{t}_{j}^{\backslash}\right) \\ &= \left\{1+\frac{\sigma_{k,j}c_0}{\sqrt{V_{k,j}^{m}}c_1}\exp\left[-\frac{(m_{k,j}^{m})^2}{2V_{k,j}^{m}}+\frac{m_{k,j}^{2}}{2\sigma_{k,j}^{2}}-\sum_{dk\in S_{k,j+1}}\frac{a_{dk}^{2}r_{k+dk,j+1}^{2}}{2\left(1-a_{dk}^{2}\right)\sigma_r^{2}}\right]\prod_{dk\in S_{k,j+1}}\sqrt{1-a_{dk}^{2}}\right\}^{-1}\end{aligned} \tag{A.48}$$

Bibliography

[1] J. Mendel, J. Kormylo, F. Aminzadeh, J. S. Lee, and F. Habibi-Ashrafi, "A novel approach to seismic signal processing and modeling," *Geophysics*, vol. 46, pp. 1398–1414, 1981.

[2] J. Kormylo and J. Mendel, "Maximum likelihood detection and estimation of Bernoulli-Gaussian processes," *IEEE Trans. Inf. Theory*, vol. 28, no. 3, pp. 482–488, 1982.

[3] J. M. Mendel, *Optimal Seismic Deconvolution: An Estimation-Based Approach.* New York: Academic, 1983.

[4] J. Goutsias and J. M. Mendel, "Maximum-likelihood deconvolution: An optimization theory perspective," *Geophysics*, vol. 51, pp. 1206–1220, 1986.

[5] K. F. Kaaresen and T. Taxt, "Multichannel blind deconvolution of seismic signals," *Geophysics*, vol. 63, no. 6, pp. 2093–2107, 1998.

[6] K. F. Kaaresen, "Deconvolution of sparse spike trains by iterated window maximization," *IEEE Trans. Signal Process.*, vol. 45, no. 5, pp. 1173–1183, 1997.

[7] Q. Cheng, R. Chen, and T. H. Li, "Simultaneous wavelet estimation and deconvolution of reflection seismic signals," *IEEE Trans. Geosci. Remote Sens.*, vol. 34, no. 2, pp. 377–384, 1996.

[8] C. P. Robert, *The Bayesian choice*. New York: Springer-Verlag, 1994.

[9] S. Geman and D. Geman, "Stochastic relaxation, Gibbs distributions and the Bayesian restoration of images," *IEEE Trans. Pattern Anal. Mach. Intell.*, vol. 6, no. 6, pp. 721–741, 1984.

[10] O. Rosec, J. Boucher, B. Nsiri, and T. Chonavel, "Blind marine seismic deconvolution using statistical MCMC methods," *IEEE J. Ocean. Eng.*, vol. 28, no. 3, pp. 502–512, 2003.

[11] M. Lavielle, "A stochastic algorithm for parametric and non-parametric estimation in the case of incomplete data," *Signal Processing*, vol. 42, no. 1, pp. 3–17, 1995.

[12] G. Celeux and J. Diebolt, "The SEM algorithm: a probabilistic teacher algorithm derived from the EM algorithm for the mixture problem," *Computational Statistics Quarterly*, vol. 2, no. 1, pp. 73–82, 1985.

[13] G. Celeux, D. Chauveau, and J. Diebolt, "Stochastic versions of the EM algorithm: an experimental study in the mixture case," *Journal of Statistical Computation and Simulation*, vol. 55, no. 4, pp. 287–314, 1996.

[14] B. Chalmond, "An iterative Gibbsian technique for reconstruction of m-ary images," *Pattern Recognition*, vol. 22, no. 6, pp. 747–761, June 1989.

[15] J. Idier and Y. Goussard, "Multichannel seismic deconvolution," *IEEE Trans. Geosci. Remote Sens.*, vol. 31, no. 5, pp. 961–979, 1993.

[16] ——, "Markov modeling for Bayesian restoration of two-dimensional layered structures," *IEEE Trans. Inf. Theory*, vol. 39, no. 4, pp. 1356–1373, 1993.

[17] A. Heimer, I. Cohen, and A. Vassiliou, "Dynamic programming for multichannel blind seismic deconvolution," in *Proc. Society of Exploration Geophysicist International Conference, Exposition and 77th Annual Meeting*, San Antonio, 23-28 September 2007, pp. 1845–1849.

[18] A. Heimer and I. Cohen, "Multichannel blind seismic deconvolution using dynamic programming," *Signal Processing*, vol. 88, pp. 1839–1851, July 2008.

[19] A. A. Amini, T. E. Weymouth, and R. C. Jain, "Using dynamic programming for solving variational problems in vision," *IEEE Trans. Pattern Anal. Mach. Intell.*, vol. 12, no. 9, pp. 855–867, 1990.

[20] M. Buckley and J. Yang, "Regularised shortest-path extraction," *Pattern Recognition Letters*, vol. 18, no. 7, pp. 621–629, 1997.

[21] A. Heimer and I. Cohen, "Multichannel seismic deconvolution using Markov-Bernoulli random field modeling," *IEEE Trans. Geosci. Remote Sens.*, to be published.

[22] D. G. Forney, "The Viterbi algorithm," *Proceedings of the IEEE*, vol. 61, no. 3, pp. 268–278, March 1973.

[23] E. A. Robinson and S. Treitel, *Geophysical Signal Analysis.* Prentice-Hall, 1980.

[24] J. M. Mendel, *Maximum-likelihood deconvolution: A Journey into Model-Based Signal Processing.* Springer-Verlag New York, 1990.

[25] K. F. Kaaresen, "Evaluation and applications of the iterated window maximization method for sparse deconvolution," *IEEE Trans. Signal Process.*, vol. 46, no. 3, pp. 609–624, 1998.

[26] C. Labat and J. Idier, "Sparse blind deconvolution accounting for time-shift ambiguity," in *Proc. IEEE Internat. Conf. Acoust. Speech Signal Process., ICASSP-2006*, vol. 3, Toulouse, France, 2006.

[27] B. Nsiri, T. Chonavel, J. Boucher, and H. Nouze, "Blind submarine seismic deconvolution for long source wavelets," *IEEE J. Ocean. Eng.*, vol. 32, no. 3, pp. 729–743, 2007.

דקונבולוציה רב-ערוצית של מידע שכבתי באמצעות שיטות MCMC

עידן רם

דקונבולוציה רב-ערוצית של מידע שכבתי באמצעות שיטות MCMC

חיבור על מחקר

לשם מילוי חלקי של הדרישות לקבלת התואר
מגיסטר למדעים בהנדסת חשמל

עידן רם

הוגש לסנט הטכניון - מכון טכנולוגי לישראל
ניסן תשס"ט חיפה אפריל 2009

המחקר נעשה בהדרכת פרופ/ח ישראל כהן ופרופ' שלום רז
בפקולטה להנדסת חשמל

הכרת תודה

אני מבקש להביע את תודתי לפרופ' ישראל כהן ופרופ' שלום רז על הנחייתם המסורה ותמיכתם במהלך כל שלבי המחקר.
תודה מיוחדת לאשתי סיגל על אהבתה ותמיכתה.

אני מודה לטכניון על התמיכה הכספית הנדיבה בהשתלמותי

תקציר

בעבודה זו אנו מציעים שני אלגוריתמים לביצוע דקונבולוציה רב ערוצית סיסמית עיוורת. דקונבולוציה רב ערוצית סיסמית נדרשת כאשר המבנה של הקרקע משוערך באמצעות שידור גל אקוסטי אל תוך האדמה ומדידת האנרגיה המוחזרת כתוצאה משינויי אימפדנס. תחת הנחות מפשטות, ניתן למדל את המדידות המתקבלות מהגלים המוחזרים כקונבולוציה מורעשת בין תמונת החזריות (reflectivity) דו ממדית ופולס אקוסטי (wavelet) חד ממדי. בעבודה זו אנו מניחים שהקרקע מכילה מספר שכבות הומוגניות ,רציפות, ופחות או יותר אופקיות. כתוצאה מכך, תמונת ההחזריות הדו ממדית תהיה רציפה, והגבולות בין השכבות המוכלים בה יופיעו בצורת קווים חלקים עם אוריינטציה שהיא בדרך כלל אופקית. ה-wavelet הסיסמי הוא אות אנכי חד מימדי המייצג את צורת הגל המתפזר דרך התווך, וההנחה היא שהוא משותף לכל טורי המידע הסיסמי. מכיוון שהמידע הסיסמי הנמדד הוא גרסה מטושטשת של תמונת ההחזריות, נעשה שימוש בדקונובולוציה על מנת להסיר את השפעת ה-wavelet וליצור תמונת החזריות משוערכת בעלת רזולוציה מוגברת, אשר מאפשרת הבחנה בין מחזירורים (reflectors) קרובים. ה-wavelet בדרך כלל אינו ידוע, לכן נדרש לבצע דקונבולוציה עיוורת על מנת לשחזר גם את ה-wavelet וגם את תמונת ההחזריות.

שיטות רבות מנצלות את העובדה שה-wavelet הוא אות חד מימדי, ומפרקות את בעיית הדקונבולוציה הרב ערוצית למספר בעיות דקונבולוציה חד ממדיות (חד ערוציות) בלתי תלויות. בעיית הדקונבולוציה החד ממדית היא קשה מאוד מכיוון שבנוכחות רעש, רצפי החזריות שונים עלולים להוביל למידע סיסמי דומה. לכן יש להשתמש במידע מקדים על רצף ההחזריות , על מנת להגביל את קבוצת הפתרונות הסבירים. רצף החזריות חד מימדי, נראה בכיוון האנכי כמו רכבת מחזירורים דלילה, כאשר כל מחזירור המופיע בה מתאים לגבול בין שתי שכבות הומוגניות סמוכות. האלגוריתם החד ערוצי עליו מבוססים שני האלגוריתמים המוצעים בהמשך, מתחשב במידע הסטטיסטי המוכל במבנה אות ההחזריות, וממדל את ההחזריות באמצעות תהליך ברנולי גאוסי (BG). עבור כל דגימה של רצף ההחזריות, מאפיין משתנה ברנולי את הנוכחות או ההיעדרות של מחזירור וכאשר קיים מחזירור ,האמפליטודה שלו היא בעלת התפלגות גאוסית. האלגוריתם מבצע דקונבולוציה עיוורת, כלומר הוא משערך את ה-wavelet, שונות הרעש ופרמטרי ההחזריות ה-BG מתוך המידע הסיסמי החד ממדי. תחילה מבוצע שיערוך maximum likelihood (ML) של פרמטרי המודל, כאשר מקסימיזציית קריטריון הסבירות (likelihood) מתבצעת באמצעות אלגוריתם ה-stochastic expectation maximization (SEM). לאחר שערוך הפרמטרים, תהליך הדקונבולוציה מתבצע באמצעות אלגוריתם ה-maximum posterior mode (MPM). אלגוריתם זה משתמש בראליזציות של רצף ההחזריות, אשר סומלצו בעזרת שיטת Markov Chain Monte Carlo (MCMC) הקרויה דוגם גיבס, על מנת לשערך את רצף ההחזריות.

שחזור תמונת החזריות דו ממדית מתוך תמונה סיסמית דו ממדית באמצעות האלגוריתם החד ממדי שתואר לעיל מתבצע על ידי החלתו על כל אחת מהעמודות של התמונה הסיסמית באופן בלתי תלוי. תהליך דקונבולוציה זה מייצר תוצאות תת אופטימליות מכיוון שהוא אינו לוקח בחשבון את התלות המרחבית בין עמודות החזריות שכנות, אשר נובעת מהמבנה הרציף והפחות או יותר אופקי של הגבולות בין השכבות. לעומת זאת, כל אחד מהאלגוריתמים המוצעים בעבודה זו מבצע את הדקונבולוציה תוך כדי התחשבות בתלות המרחבית בין עמודות המידע הסיסמי. שני האלגוריתמים המוצעים מבוססים על המודל ה-I Markov Bernoulli Gaussian (MBG) של תמונת ההחזריות הדו ממדית, המהווה הרחבה דו ממדית של הייצוג ה-BG החד ממדי ומתחשב במבנה השכבתי של תמונת ההחזריות הדו ממדית. מודל ה-MBG I מורכב משני חלקים: ה-Markov Bernoulli random field (MBRF) ושדה אמפליטודות המחזירורים. ה-MBRF שולט על המאפיינים הגאומטריים של תמונת ההחזריות. אמפליטודות המחזירורים בלתי תלויות בכיוון האנכי, בעלות התפלגות גאוסית ותלויות בקורלציה בין מחזירורים בטורים שכנים, הנקבעת על ידי הגאומטריה המקומית של השכבות. מכיוון שהדקונבולוציה היא עיוורת, ה-wavelet, שונות הרעש ופרמטרי מודל ה- MBG I אינם ידועים ולכן יש לשערך אותם. אנו משערכים פרמטרים אלה באמצעות אלגוריתם ה- SEM ומתוך תמונת החזריות המשוחזרת על ידי החלת אלגוריתם ה-MPM על כל אחד מטורי המידע הסיסמי הנתון. לאחר שערוך הפרמטרים כל אחד מהאלגוריתמים המוצעים מבצע את הדקונבולוציה בצורה איטרטיבית, טור אחרי טור.

האלגוריתם המוצע הראשון משתמש בכל איטרציה בגרסה מורחבת של אלגוריתם ה-MPM אשר משערכת את טור ההחזריות הנוכחי מטור המידע הסיסמי המתאים ושערוך של טור ההחזריות הקודם. אלגוריתם ה-MPM הזה משערך את משתני ה-MBRF והאמפליטודה המתאימים לטור ההחזריות הנוכחי בשני שלבים. תחילה הוא משתמש בדוגם גיבס על מנת לסמלץ ראליזציות של משתנים אלו על ידי דגימה איטרטיבית מתוך ההתפלגויות המותנות שלהם, אשר תלויות בשערוך של טור ההחזריות הקודם. לאחר מכן מתרחש שלב החלטה בו משתני ה-MBRF והאמפליטודה נקבעים מתוך הראליזציות שלהם. תחילה נקבע כל אחד ממשתני ה-MBRF על ידי מיצוע הראליזציות שלו והשוואתן לסף. אחר כך נקבעים משתני האמפליטודה על פי הערכים של משתני ה-MBRF.

האלגוריתם המוצע השני, מהווה הרחבה של האלגוריתם הראשון, אשר לוקחת בחשבון בתהליך הדקונבולוציה את התלות של כל טור החזריות גם בטור הקודם לו וגם בטור הבא. בכל איטרציה טור ההחזריות הנוכחי והבא משוערכים בו זמנית, מכיוון שלא קיים שערוך של הטור הבא מאיטרציות קודמות. באופן זה, התלות בין טורי ההחזריות הנוכחי והבא נלקחת בחשבון כאשר הטור הנוכחי משוערך. השערוך עצמו מתבצע בעזרת גרסה מורחבת יותר של אלגוריתם ה-MPM אשר קובעת בו זמנית את טורי ההחזריות הנוכחי והבא מטורי המידע הסיסמי המתאימים והשערוך של טור ההחזריות הקודם. גם כאן פועל אלגוריתם ה-MPM בשני שלבים. תחילה נעשה שימוש בדוגם גיבס על מנת לסמלץ ראליזציות של משתני ה-MBRF והאמפליטודה המתאימים לטורי ההחזריות הנוכחי והבא, על ידי דגימה איטרטיבית מתוך ההתפלגויות המותנות שלהם. לאחר מכן משתני ה-MBRF והאמפליטודה נקבעים מתוך הראליזציות שלהם בשלב החלטה הדומה לזה המתואר לעיל. מתוך השערוכים המתקבלים, רק

השערוך של טור ההחזריות הנוכחי נשמר. השערוך של טור ההחזריות הבא נזרק, מכיוון שטור זה ישוערך מחדש באיטרציה הבאה, מהשכנים הקודם והעוקב שלו.

שני אלגוריתמי הדקונבולוציה הרב ערוצית המוצעים מוחלים על מידע סינטטי ואמיתי. עבור המידע הסינטטי הם מפיקים תוצאות רציפות יותר, המכילות פחות גילויים כוזבים וקרובות יותר באופן כללי לתמונת ההחזריות המקורית מאשר התוצאות המתקבלות באמצעות אלגוריתם הדקונבולוציה החד ערוצית המתואר לעיל. גם עבור מידע אמיתי מפיקות השיטות המוצעות תוצאות רציפות יותר, בהן השכבות מזוהות בצורה טובה יותר מאשר התוצאות המתקבלות בשיטת הדקונבולוציה החד ערוצית. שני האלגוריתמים המוצעים אף מושווים אחד לשני. האלגוריתם השני אשר משתמש ביותר מידע מטורי המידע הסיסמי השכנים בתהליך הדקונבולוציה של כל טור מידע סיסמי מדגים גילוי טוב יותר של השכבות מאשר האלגוריתם הראשון, עבור מידע סינטטי ואמיתי.